Australian Government
Bureau of Meteorology

The Centre for Australian Weather and Climate Research
A partnership between CSIRO and the Bureau of Meteorology

CSIRO

High Resolution Met-Ocean Modelling for Storm Surge Risk Analysis in Apia, Samoa – Final Report

Ron Hoeke, Kathy McInnes, Julian O'Grady, Felix Lipkin and Frank Colberg

CAWCR Technical Report No. 071

June 2014

www.cawcr.gov.au

High Resolution Met-Ocean Modelling for Storm Surge Risk Analysis in Apia, Samoa – Final Report

Ron Hoeke, Kathy McInnes, Julian O'Grady, Felix Lipkin and Frank Colberg

Centre for Australian Weather and Climate Research (CAWCR), Bureau of Meteorology, Melbourne, Australia, 3008

CAWCR Technical Report No. 071

June 2014

ISSN: 1835-9884

National Library of Australia Cataloguing-in-Publication entry

Authors: Ron Hoeke, Kathy McInnes, Julian O'Grady, Felix Lipkin and Frank Colberg

Title: High resolution met-ocean modelling for storm surge risk analysis in Apia, Samoa.

ISBN: 9781486303212

Notes: Includes bibliographical references and index.

Subjects: Storm surges--Samoa--Apia--Mathematical models.

Storm winds--Samoa--Apia--Mathematical models.

Wind waves--Samoa--Apia--Mathematical models.

Sea level--Samoa--Apia--Mathematical models.

Cyclones--Samoa--Apia.

Dewey Number 551.463099614

Enquiries should be addressed to:

Ron Hoeke
Centre for Australian Weather and Climate Research:
A partnership between the Bureau of Meteorology and CSIRO
GPO Box 1289, Melbourne
Victoria 3001, Australia

Ron.Hoeke@csiro.au

Copyright and Disclaimer

All images reproduced in grayscale. A colour version of CAWCR Technical Report No.071 is available online: http://www.cawcr.gov.au

Contents

List of Figures

List of Tables

EXECUTIVE SUMMARY

Under a partnership between the Government of Australia and the Government of Samoa, Australian development assistance is supporting the Samoan Parliament Complex Redevelopment Project (SPCRP). A recent study by Hay and Hartley (2013) commissioned in support of this project assessed the climate risk and adaptation options of the SPCRP and determined that the greatest risk to the Parliament Complex being located on the Mulinu'u Peninsula in Apia was due to inundation as a result of a cyclone-related storm surge. Under the Pacific-Australia Climate Change Science and Adaptation Planning (PACCSAP) Program, Australia has commissioned CSIRO to better quantify this risk by undertaking high resolution modelling of the local sea level response associated with tropical cyclone storm surges in the Apia Harbour region.

Fig. ES1 Mulinu'u Peninsula, Apia

In this study, hydrodynamic models have been used to estimate extreme values of sea level arising from astronomical tides, storm surge (i.e. inverse barometer effect and wind setup), and nearshore wind-wave dissipation and breaking at the coast. Simulating (modelling) these processes, especially those related to wind-wave generation and breaking (such as coastal wave setup and wave run-up) require a range of spatial extents and resolutions. High-resolution topography and bathymetry of the Apia area, acquired through a PACCSAP-funded Light Detection and Ranging (LiDAR) survey, provided the crucial spatial detail needed by the models used in this study. The study also utilized other PACCSAP research products, including the findings of a study addressing tropical cyclone storm tide risk across the Samoan archipelago, projections of future sea level rise and a historical wave model (hindcast) for the Pacific region.

The present study estimates return periods of storm tides (defined here as the combination of astronomical tides, inverse barometer effect and wind setup) caused by tropical cyclones in Samoa, and builds into those estimates the additional influence of tropical cyclone generated wind-waves. To manage the computational demands required to undertake a full joint-probability analysis of storm tides, including wave effects, a 'limited ensemble' approach was adopted in this study. A sample of ten statistically generated (synthetic) cyclone events that

produced storm tide heights that matched those assessed as 20-year, 50-year and 100-year storm tides were modelled at archipelago to reef scales using wave and circulation models in order to incorporate the additional effect of waves on coastal extreme sea levels, currents and inundation. From this range of simulated wave heights an average value and range (uncertainty) of the associated storm tide and wave height contribution (i.e. wave setup and run-up) was calculated.

The time horizons considered in this study were 1990 (the baseline) and 2030, 2055 and 2090. The sea-level rise projections for Samoa used in this study are the 95% range of a medium-emissions future scenario (A1B, Nakicenovic, et al., 2000), with increases of 0.14, 0.30 and 0.57 m for 2030, 2055 and 2090 respectively and relative to 1990.

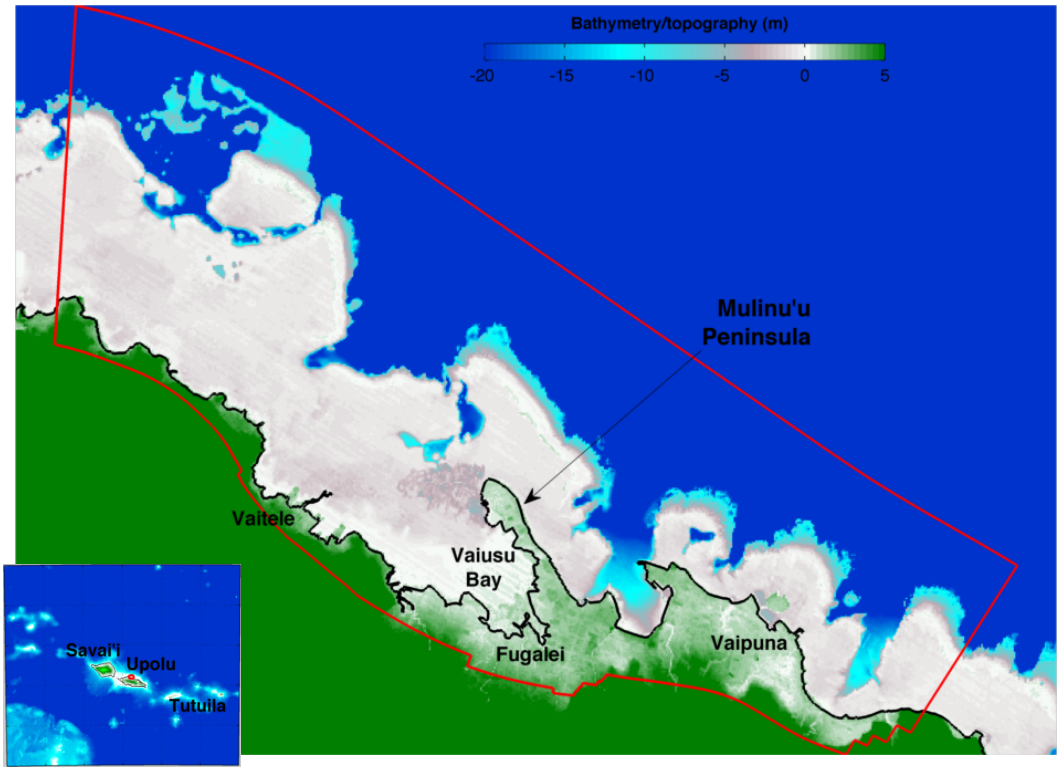

Fig. ES2 Diagram showing the region covered by the Apia hydrodynamic model (outlined in red). Bathymetry and topography were derived primarily from the LiDAR survey and shading indicates levels (in m) relative to mean sea level. The region covered by the Peninsula models is shown in the bottom left hand inset.

A hierarchy of models at different scales were used in this study: the "Archipelago Models", the "Apia Model" and the "Peninsula Model". The Archipelago Models consist of wind-wave and circulation (flow) models (see inset of Fig. ES2) and were implemented over the region spanning 184° to 192°W and 10°to 16°S at 5 and 1 km resolutions, respectively, with a 1 km "nested" wind-wave model just encompassing the islands of Savaii, Upolu and Tutuila. The Apia Model incorporated all of coastal Apia (Fig. ES2) with a variable resolution grid, with highest resolution of around 10m over Mulinu'u Peninsula. This model simultaneously simulated storm-tide, phase-averaged wave propagation, breaking, and wave setup at hourly timescales. The 1-dimensional non-hydrostatic Peninsula Model was implemented along a section from the seaward reef edge and across the Mulinu'u Peninsula at 0.5 m resolution. This model was used to simulate instantaneous wave heights, wave run-up and seawall

overtopping, as well as infragravity waves, which were shown to be important contributors to wave run-up and overtopping.

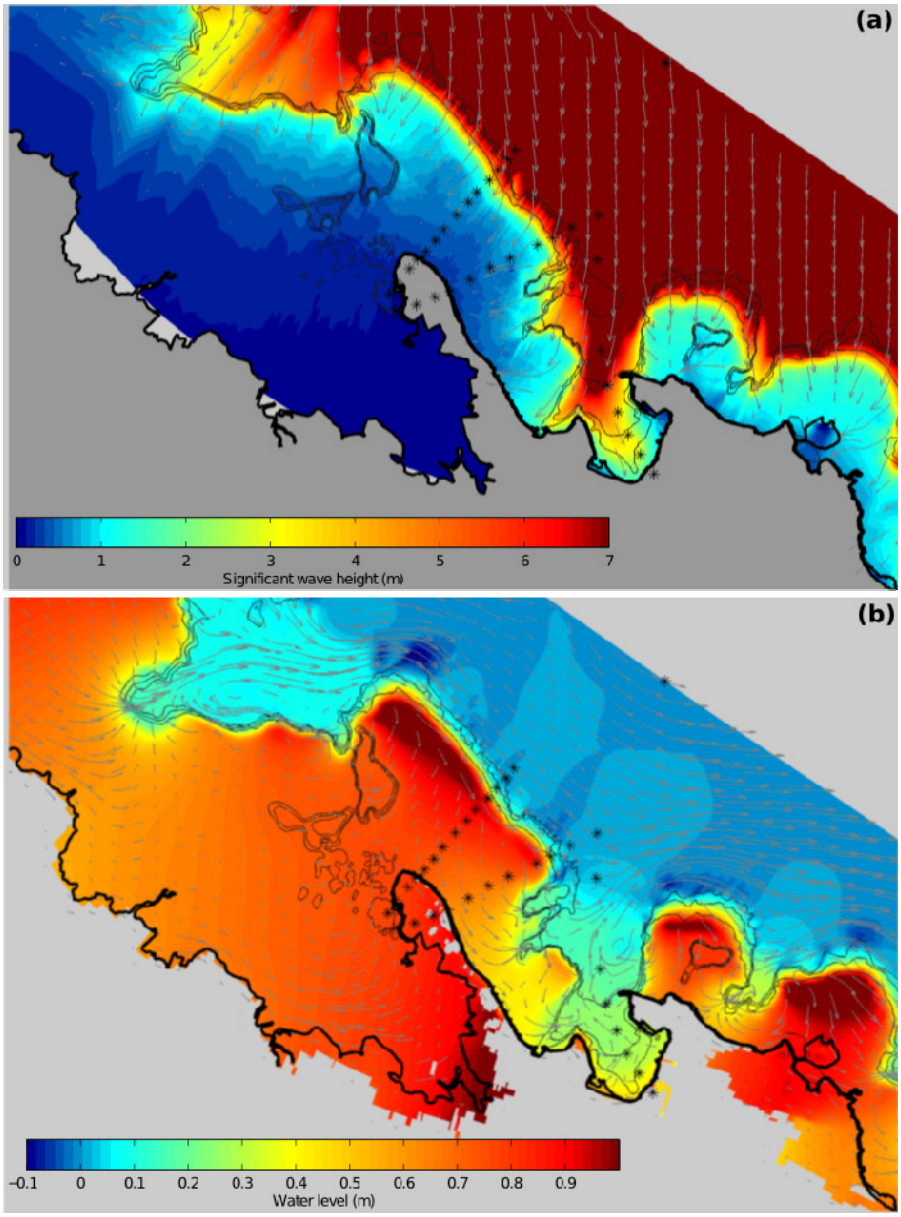

Fig. ES3 Apia Model output near the peak of local water levels during Cyclone Ofa: (a) significant wave height and peak wave direction (arrows); (b) non-tidal water levels and depth-averaged current vectors (arrows).

Model results highlight that the sea-level response under cyclone conditions is complex and highly variable along the coastline of Apia due to the effects of wave breaking and energy dissipation that occurs over the complex fringing reefs fronting the Apia foreshore. However, consistent patterns of sea-level and wave setup response were evident from the simulations, an example of which is illustrated using modelled significant wave heights and water levels arising from Cyclone Ofa (Fig. ES3). Significant inundation of the peninsula and adjacent coastline in Vaiusu Bay is evident in the simulation, consistent with anecdotal information about the extent of the flooding during this cyclone. Overland flooding is also evident at

Vaipuna to the east of Apia Harbour. Mulinu'u Peninsula is particularly exposed to wave setup due to the presence of fringing reefs to the northeast. Vaiusu Bay to the west of Mulinu'u Peninsula is vulnerable to elevated sea levels due to wind setup.

Under the synthetic cyclone conditions and assuming median wave conditions assessed from the 'limited ensemble' method for the 20-, 50- and 100-year storm tides, it is found some degree of inundation of the Peninsula was present for all scenarios considered. Inundation in the Apia Model tended to occur from the western (Vaiusu Bay) side of the Peninsula and increasingly covered the entire peninsula for the higher storm surge levels (i.e. the 1-in-100 year event) and future sea-level rise scenarios. This was primarily due to the high wind setup that tended to occur across Vaiusu Bay's shallow bathymetry during storm tide conditions. However, significant wave heights simulated by the Apia Model were in the range of 1-3 m in front of the seaward facing seawall for all scenarios considered, while wave heights within Vaiusu Bay were less than 0.5m. Thus overtopping of the seaward seawall by individual waves (not explicitly modelled by the Apia Model) is likely an additional significant driver of inundation, along with the primarily wind-driven inundation from Vaiusu Bay (which is explicitly modelled by the Apia Model). The Peninsula Model confirmed this, as it indicated that individual waves could successively overtop the seawall fronting the Mulinu'u Peninsula, leading to significant inundation from the ocean side of the peninsula in higher wave conditions associated with 50- and 100-year storm tides.

The relative importance of inundation of the Mulinu'u Peninsula due to wind setup in Vaiusu Bay (as indicated by the Apia Model) and wave overtopping of the seawall on the eastern side (as indicated by the Peninsula Model) is dependent on the specific details of particular storms, such as track, intensity and radius of maximum winds. Inundation from both processes is highly likely in 50- and 100-year storm tides, which combine high incident wave fields with strong north-westerly winds, as occurred in several synthetic cyclone cases. While uncertainty remains around exactly which combination of storm characteristics will result in the most extreme overall water levels, ensemble model results suggest that conditions tend to be most severe when a storm with a large radius of maximum winds approaches Apia from the north, has a medium forward speed and passes Apia just to the east.

Water levels under 1990 (baseline) conditions at a location in front of the sea wall from the Peninsula Model are compared to earlier studies (Fig. ES4). Results indicate that wave setup more than doubles the water levels that occur due to the storm tide only. The median (50^{th} percentile) water level from the model is taken to represent storm tide+wave setup. The breaking of individual waves against the sea wall produces run-up and sea levels that are temporarily higher than the average values. These extreme heights, referred to as maximum heights, are defined as the average of those that are attained 2% of the time during each storm event simulation, and represent the combined sea level due to storm tide, wave setup and run-up. Under all return periods considered, these transitory extreme sea levels exceed the height of the seawall, which is about 2.4-2.5 m above mean sea level. This means that during cyclone events the seawall will experience overtopping, and the amount of overtopping increases with more extreme storm events (i.e. longer return periods).

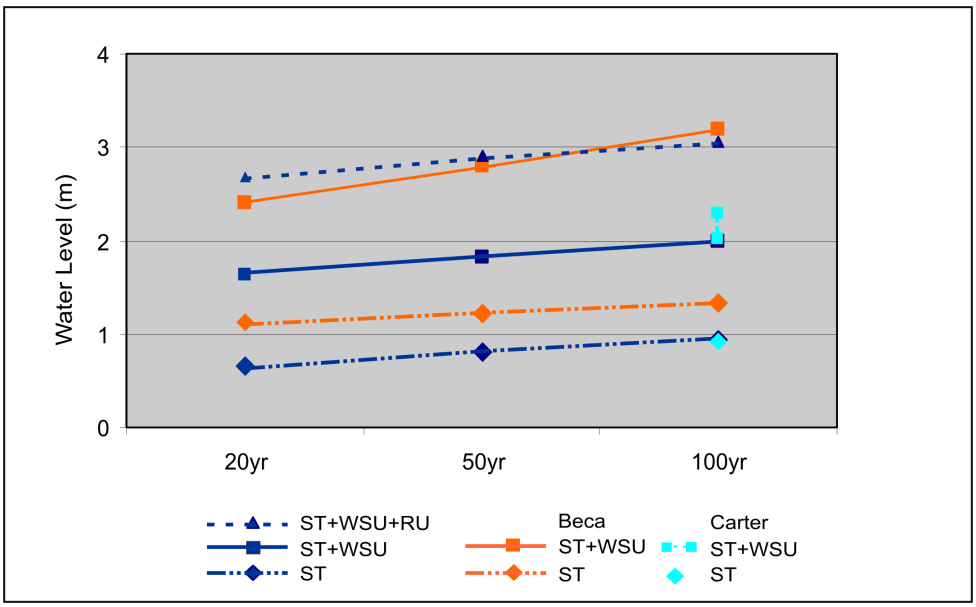

Fig. ES4 Comparison of modelled water levels for 20-, 50- and 100-year return period levels for baseline (current climate) sea level in the present study (dark blue symbols) with those estimated in previous studies. ST refers to storm tide, WSU refers to wave setup and RU refers to run-up. Values estimated by Beca (2001) and Carter (1987) are shown in orange and light blue respectively. Water levels are relative to the 1973 MSL datum. Note that the ST+WSU+RU water levels plotted correspond to the mid-range estimates of the Peninsula Model.

The results of an earlier study by Carter (1987) estimated a 1-in-100 year storm tide level of 0.92 m, very close to that estimated for the present study (Fig. ES4). Assuming an incident wave height of 11.3 m, a period of 13.6 s and wave length of 288 m, Carter estimated wave setup to be 1.11-1.40 m, using two different empirical approaches, the lower value of which is close to the value determined in this study. The storm tide estimates of Beca (2001) for 20 to 100-year levels are around 50% higher than those modelled in the present study. The higher storm tide estimates are a result of the choice to combine estimated values of storm surge height with a tidal value of 0.5 m above mean sea level, in other words a maximum spring tide height. However the joint probability approach used in this study shows that the return period of a significant tropical cyclone coinciding with a maximum spring tide is much longer than the return periods considered in this study. Consistent with this, Carter (1987) assumed a lower tidal contribution of 0.2 m. Values of wave setup in the study of Beca (2001) are also considerably higher and are more closely aligned with the maximum values estimated in the present study that are reached around 2% of the time due to the additional effect of wave run-up. The higher results of Beca (2001) are most likely due to the simple empirical approach used to estimate wave setup, although it should be noted that the storm tide+wave setup of Beca (2001) fall below the mid-range and upper estimates (see below) of storm tide+wave setup+wave run-up calculated by this study.

Indicative values of sea level and currents behind the sea wall under baseline and future sea level rise scenarios were also determined (Fig. ES5). The median values (50th percentile) from the Peninsula Model were consistent with water levels simulated by the Apia Model and were considered to be a *lower estimate* since they do not account for wave run-up, overtopping or the presence of infragravity waves. The additional water level height and current speed due to run-up and overtopping is estimated from the Peninsula Model and is added to the *low estimate* results to produce a *mid-range estimate*, considered to be the most likely. To account

for uncertainty in the model results due to the absence of observational data for model calibration, an *upper estimate* of sea level is obtained by using the version of the Peninsula Model in which model parameter settings were combined to favour more extreme inundation. For a 1-in-100 year storm tide the *mid-range estimate* of sea level is around 2.5 m in 1990, increasing to around 2.8 m in 2090 and currents are around 2.0 ms^{-1} in 1990 and increase to 2.5 ms^{-1} in 2090 conditions

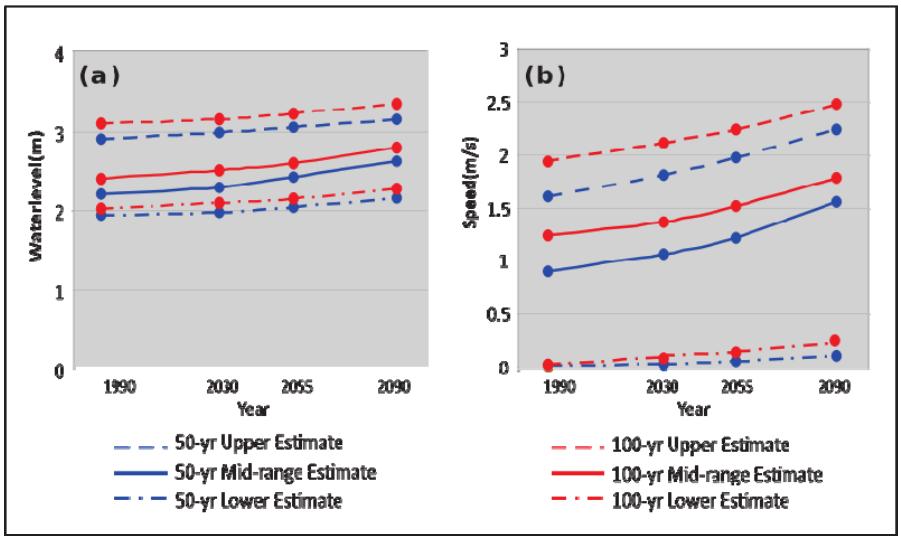

Fig. ES5 Average and maximum (a) sea levels and (b) current speeds attained on the landward side of the seawall under future scenarios of sea level rise for 1-in-50 year (50-yr) and 1-in-100 year (100-yr) return intervals. The *lower estimate* values are derived from the Apia Model since they do not include the effects of transient wave activity (i.e. wave run-up and overtopping). The *mid-range estimate* is derived by adding to the Apia Model results the difference in the 50th and 98th percentile heights estimated from the Peninsula Model to account for the effects of transient wave activity. The *upper estimate* is derived in the same way as the *mid-range estimate* but using the Peninsula Model values where the parameter settings favoured more extreme inundation. Water levels are relative to the 1973 MSL datum.

Modelling of tropical cyclone storm tides with the Apia Model highlights the areas of Apia that are at risk of inundation and shows that the Mulinu'u Peninsula is particularly vulnerable. The inland extent of the modelled inundation is shown in Fig. ES6 for the 50- and 100-year storm tides under the different scenarios of sea-level rise. Model estimates suggests that where a 1-in-50 year storm tide under baseline conditions would have caused only partial inundation of the western side of Mulinu'u Peninsula, a 1-in-100 year storm tide would completely inundate the peninsula. By 2055, increases in sea level would result in a 1-in-50 year storm tide completely inundating the peninsula as well. Other areas of Apia that are at considerable risk of flooding during tropical cyclone storm tides include the coastline from Fugalei to Vaiusu to the west of Mulinu'u Peninsula and Vaipuna on the eastern side of town under higher sea level rise scenarios. Model results indicate that for a 1-in-100 year storm tide including future projected sea level rise, maximum sea levels on Mulinu'u Peninsula will likely be 2.6 m *(mid-range estimate)* to 3.2 m *(upper estimate)* above current mean sea level in 2055. It should be noted that overtopping of the Apia seawall away from the Mulinu'u Peninsula was not directly modelled and therefore remain unquantified. This risk may be significant in Apia Harbor where the Apia Model indicates significant wave penetration closer to shore compared to surrounding areas (e.g. Fig. ES3a).

The results obtained from this study have been based upon the best available science on climate change and coastal processes, using state-of-the-art numerical modelling in complex reef environments together with high resolution LiDAR data. The results presented here effectively identify areas of Apia most at risk of inundation from tropical cyclone storm surge and waves, helping to constrain the uncertainty around actual inundation processes and levels. It should be noted however that the numerical models contain approximations for the actual physical environment. While every effort has been made to benchmark these models against available observations, there are no observations around the Peninsula, or wave measurements in Apia. Furthermore, the methods applied to derive the storm tide return period estimates are also based on assumptions due to limited historical records and measurements of tropical cyclones. This necessarily leads to uncertainties in the results and these should be factored in to any use of the results for particular applications.

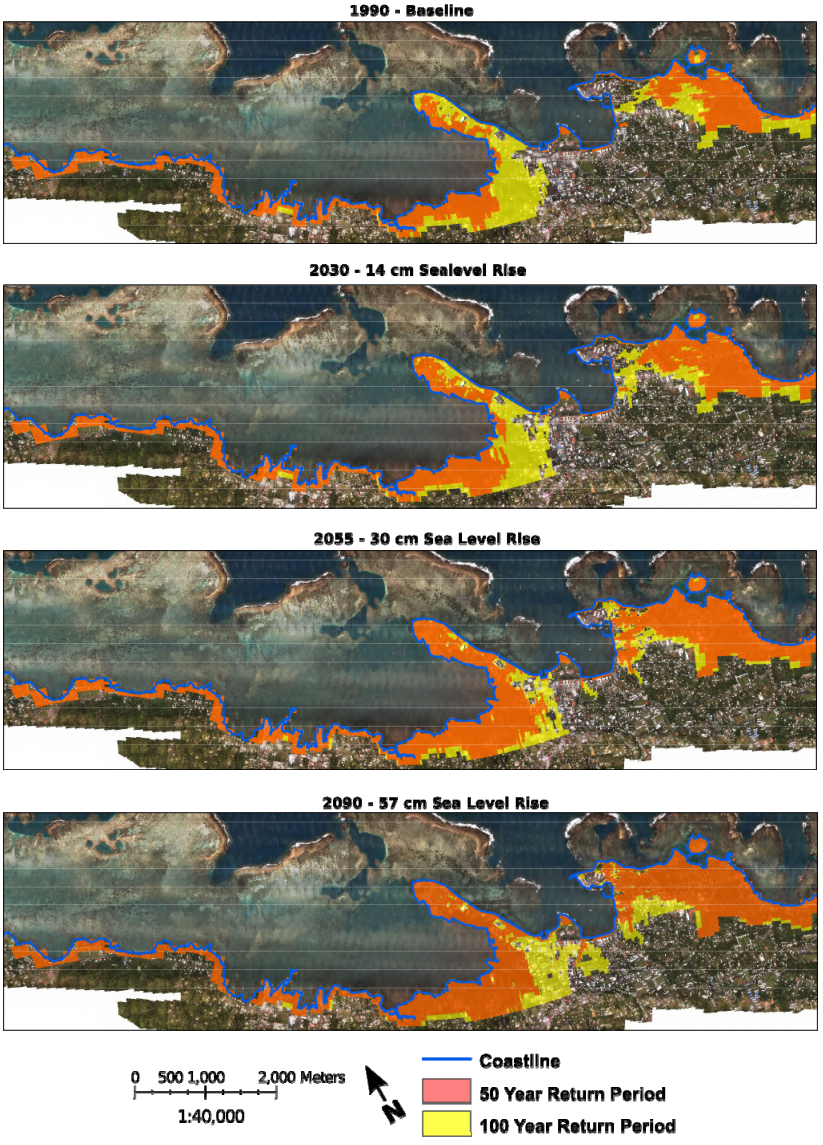

Fig. ES 6 The estimated area inundated by the Apia Model (storm tide and wave setup), for 50 year and 100 year return period storms under 1990 (baseline) and 2030, 2055 and 2090 future sea level scenarios.

1. INTRODUCTION

The purpose of this study is to investigate extreme water levels and associated currents and inundation along the coast of Apia and especially in the vicinity of the Mulinu'u Peninsula (Fig. 1) under conditions associated with tropical cyclones. This is to provide relevant information for the Samoan Parliament Complex Redevelopment Project (SPCRP) that is being supported through a partnership between the Government of Australia and the Government of Samoa. The location for the Parliament redevelopment is towards the northern end of the Mulinu'u Peninsula (Fig. 1). A number of studies have identified the peninsula's vulnerability to storm surge inundation (e.g. Hay and Hartley, 2013), particularly under projected future sea level rise. Hay and Hartley (2013) recommended a detailed assessment of current and projected future storm surge risk be undertaken for the Apia area.

As part of the Pacific-Australia Climate Change Science and Adaptation Planning (PACCSAP) Program, the Department of Industry, Innovation, Climate Change, Science, Research and Tertiary Education (DIICCSRTE) funded the CSIRO to model the maximum water level heights and associated flow velocities for one in 20, 50, and 100-year storm surge events at the Mulinu'u peninsula, Apia, and surrounding urban regions for present day conditions as well as those projected for 2030, 2055 and 2090.

The current study draws on findings from previous PACCSAP-funded efforts by CSIRO to model storm-tide heights for the entire Samoa archipelago using a synthetic tropical cyclone approach (e.g. McInnes et al. 2014). The present study assesses extreme sea levels at considerably higher resolution than that study and considers the effects of surface wind-wave processes such as wave setup and wave run-up, and evaluates instantaneous maximum wave height and current velocities. This modelling work is made possible by the recent collection and processing of high-resolution light detection and ranging (LiDAR) topography and bathymetry of the Apia area, also funded under PACCSAP.

2. BACKGROUND

2.1 Extreme Sea Levels

Storm surges are caused by the inverse barometer effect (IBE) and surface wind stresses acting over coastal seas (wind setup). At the coast, tropical cyclone-induced storm surges tend to be localised and concentrated in the region of maximum onshore winds close to the cyclone centre. The severity of storm surges is influenced by cyclone intensity and movement in relation to the impacted coastline. Coastal bathymetry also influences storm surges with wide and shallow continental shelf regions experiencing greater wind setup than narrow continental shelf regions and islands (e.g. Kennedy et al., 2012; Hoeke et al., 2013a).

The severity of the extreme sea levels arising from storm surges is also influenced by other variations in sea level that operate on time scales that vary from hours to years. The combination of sea levels arising from storm surges together with astronomical tides is commonly referred to as a storm tide. A further increase to coastal sea levels can occur due to

wave breaking processes, which produces wave setup and run-up (see Fig. 2). Wave breaking processes are highly localized and strongly dependent on the coastal bathymetry and coastline orientation with respect to wave approach (Kennedy et al., 2012; Hoeke et al., 2013a).

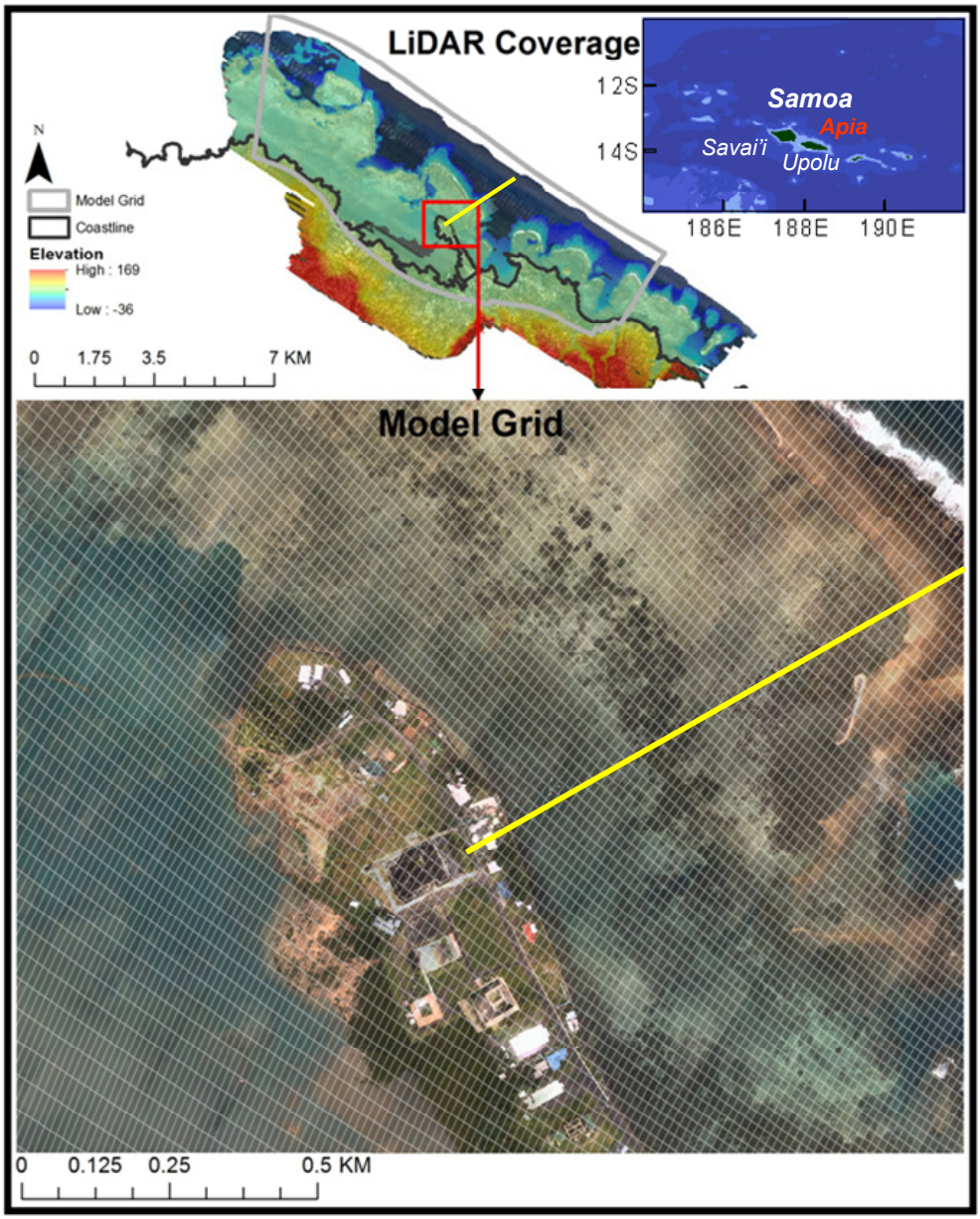

Fig. 1 Top right: the location of Apia (red rectangle) in Samoa. Top: The extent of the LiDAR data coverage around Apia with grey mesh indicating the extent of the Apia hydrodynamic model grid coverage. Bottom: a magnified view of the northern tip of the Mulinu'u Peninsula showing the resolution of the hydrodynamic model mesh over this region. The yellow line represents the centre of the 1-dimensional Peninsula hydrodynamic model.

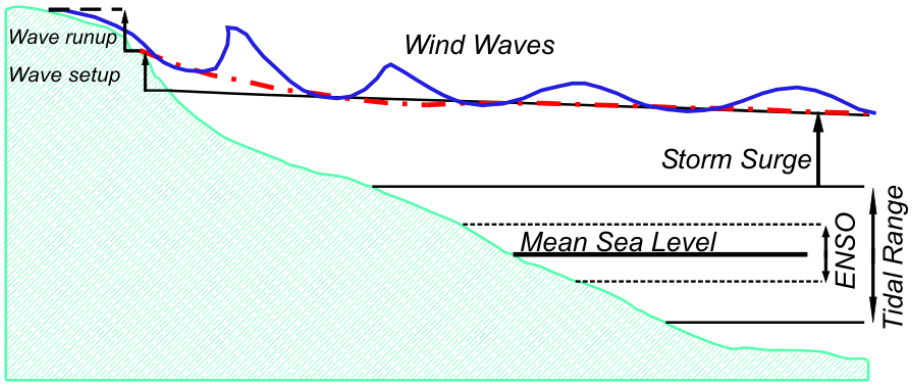

Fig. 2 The contributions to sea level due to tides, storm surge and wind-generated waves.

As well as weather-related variations to sea levels, variations can occur due to steric effects and changes in atmospheric circulation patterns that operate on seasonal and interannual time scales (e.g. Merrifield et al., 2007; Australian Bureau of Meteorology and CSIRO, 2011). El Nino Southern Oscillation (ENSO) is a major driver of such interannual variability (Church et al., 2006; Walsh et al., 2012).

In terms of measured sea level at the location of tide gauges, it is important to note that short-term, wave-induced increases in sea levels are usually minimal due to the typical location of tide gauges in deeper water within sheltered harbours (see for example Hoeke et al, 2013a). This is the case for the Apia tide gauge, which is located on the eastern side of Apia Harbour.

The complexity of the various extreme sea-level drivers interacting with the steep and complex bathymetry typical of island fringing reef environments (such as found in Samoa) means that simple empirical engineering approaches may be insufficient to accurately estimate extreme water levels, and especially nearshore hydrodynamics (e.g. currents and waves, Taebi, et al. 2012; Hoeke, et al. 2013b). Generally a modelling approach is needed, using either physical scale models or computer-based numerical models. The last decade has seen great advances in both computing power and the application of numerical modelling techniques to nearshore hydrodynamics. Complex numerical models are increasingly used to understand and predict nearshore hydrodynamic phenomena such as storm surge, wave setup and wave run-up.

2.2 Historical Data and Analysis

In this section, an analysis of available relevant historical cyclones and datasets of tide and wave information is undertaken to provide broad contextual information on the contributions to extreme sea levels for Samoa. The findings of this analysis are discussed further in subsequent sections describing the modelling methodology used in this study.

2.2.1 Historical Cyclones and their Impacts

For the purposes of testing the suite of models used in this study, a brief review of historical tropical cyclones that have affected Samoa over approximately the last 25 years (for which

reliable track information exists) is given. The tracks of these cyclones and other relevant information are provided in Fig. 3. Two of the cyclones (Ofa and Val) occurred before the establishment of the tide gauge in Apia harbour. However, the others occurred after this time. Measured sea levels and calculated non-tidal residuals (water level minus predicted tide) for Tui and Heta are shown in Fig. 4. Some of these cyclones are later used to validate the performance of the wave and hydrodynamic models. Note that although the track for cyclone Evan is shown, information about this event was not available at the time of undertaking this study and so it was not used for model validation.

Cyclone Tui was a relatively weak cyclone did not drop below 990 hPa. Nevertheless, it travelled on a northwest to southeast path between Savai'i and Upolu and therefore produced winds with a strong onshore component, favourable for wind setup, along the northeast coast of Upolu in the vicinity of Apia. Sea level residuals indicate an increase in water level of just over 0.2 m early on the 26th January 1998 (Fig. 4a). This contributed to total water levels of just over 0.7 m.

Cyclone Heta travelled on a north-south trajectory a little over 200 km to the west of Apia. The cyclone intensity dropped to 915 hPa as it crossed Apia's latitude. The maximum sea level residuals were 0.3 m, and since this occurred close to a neap high tide the maximum total water level reached almost 0.7 m.

Anecdotal and post-surge survey data provides information on the severity and nature of the impacts caused by tropical cyclones Ofa and Val. Cyclone Val is reported to have been more damaging because of its longer duration and high winds, whereas much of the destruction during Ofa was caused by waves and high water levels (Solomon, 1994). Ofa is reported to have produced deep water wave heights of 7.5 m and a maximum water level of 1.6 m which resulted in 0.5 m of submergence at the Apia Observatory (Rearic, 1990; Carter, 1991). These reports, though providing only qualitative comparisons to the modelling outputs for the most part, have been used to assess and validate the models and results presented in this study wherever possible.

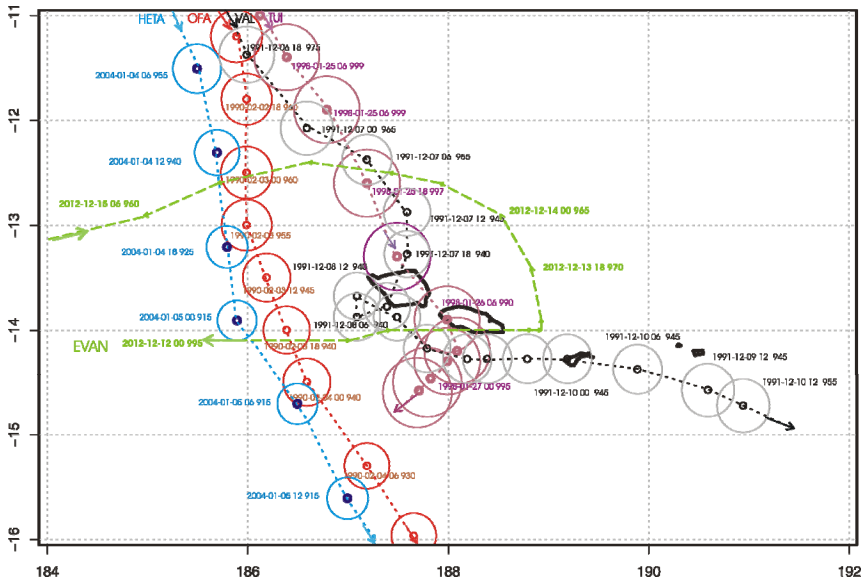

Fig. 3 Cyclone tracks for cyclones Heta, Val, Ofa and Tui. The dates, hours and minimum central pressure of the cyclones are indicated. Cyclone track information was obtained from *www.ncdc.noaa.gov/ibtracs/* and radius of maximum winds based on the relationship of Kossin (2007) (see appendix A). The track of cyclone Evan, not available at the time of undertaking this study, is also shown in green.

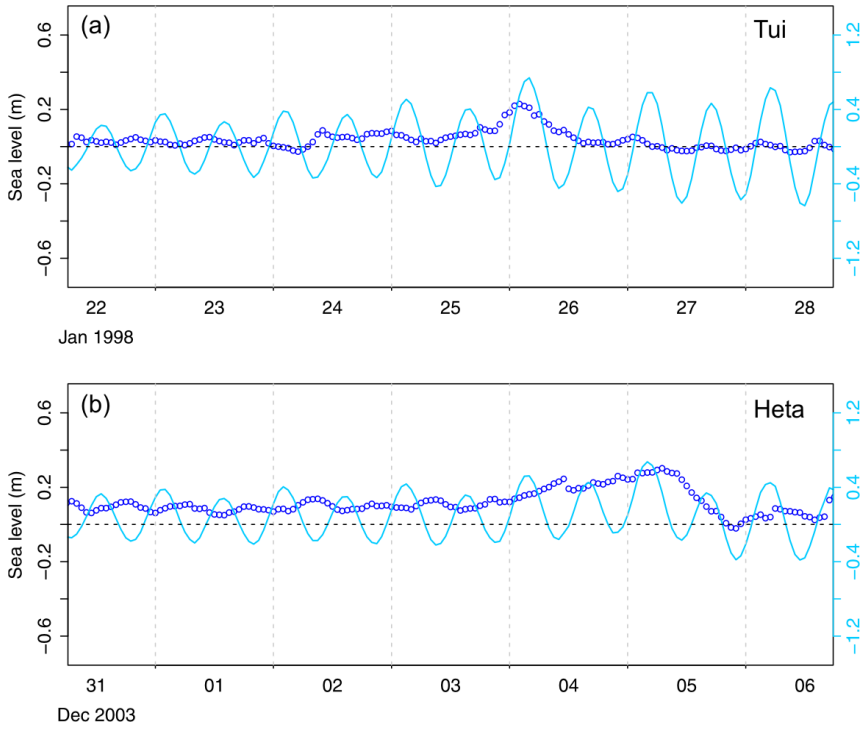

Fig. 4 Measured water levels at the Apia Tide gauge (light blue) and de-tided sea level residuals (dark blue circles) during (a) Cyclone Tui and (b) Cyclone Heta. Dates (in UTC) are shown on the bottom axis, the scale for the de-tided residuals (dark blue) is on the left vertical axis and measured total water level scale (light blue) is on the right hand vertical axis.

2.2.2 Tide Gauge Analysis and Extreme Sea Level Climatology

Hourly tide gauge data from the Australian Bureau of Meteorology's South Pacific Sea Level and Climate Monitoring Project (http://www.bom.gov.au/pacificsealevel/) for all available years (1993 – 2013) was sourced for Apia Harbour. Prior to analysis, the tide gauge water levels were adjusted to a zero bias with respect to a global sea-surface height reconstruction (SSHR) (Church and White, 2011). A common datum of zero-mean between the years 1990-1995 (a period with relatively minimal ENSO extremes) was used for both tide gauge water levels and SSHR. Harmonic analysis and prediction using exact nodal satellite corrections was carried out using Utide software (Codiga, 2011). Detrended sea level maxima were fitted to a generalized Pareto distribution (GPD) (Fig. 5; black curves). The extreme water levels generated by simulating storm tides forced by a stochastic cyclone sampling approach (synthetic cyclones) were also fitted to a GPD (Fig. 5; blue curves) using a similar approach to McInnes, et al. (2014), but for the Samoa region (see following sections and Appendix A).

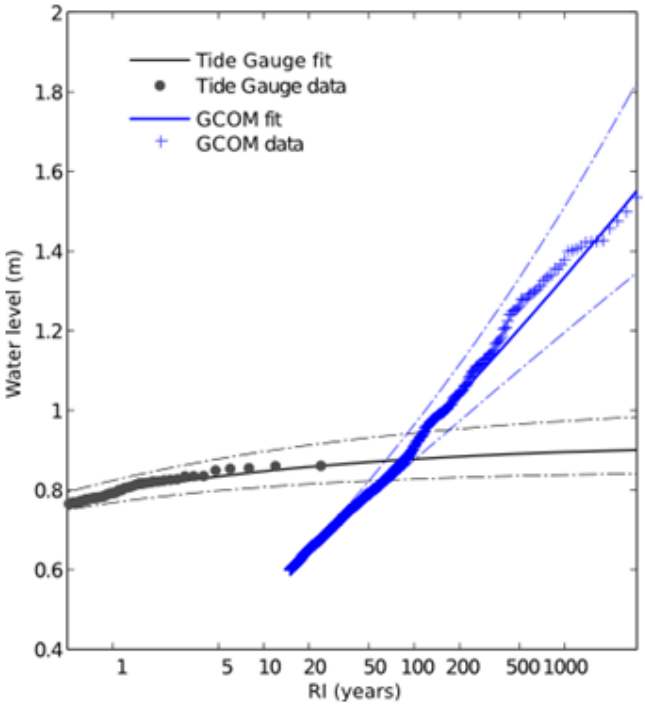

Fig. 5 Return intervals (RIs) of water level events, determined from analysis of the Apia Harbour tide gauge (black). Also shown are the return periods estimated from the synthetic cyclone storm surge (GCOM) simulations (blue). Dotted lines indicate the 95% confidence intervals.

The two curves have a markedly different shape. The location, as well as the relatively short duration of tide gauge record (~20 years), results in the data being dominated by mainly tidal extremes, with interannual variability in sea levels also playing a role. The return period curve based on the modelled tide and synthetic cyclone storm surges is steeper and attains higher sea levels at longer return periods. However at shorter return periods (i.e. 50 years and shorter), the storm tide heights are typically lower than the equivalent heights evaluated from the tide gauge observations. This is to be expected because: cyclones are statistically rare

events, with an average rate of occurrence in the Samoa region of about 1 cyclone every 7 years and their chances of coinciding with a spring high tide are low. The length of the tide gauge record would have to be significantly longer to robustly sample more extreme storm tides that could arise from tropical cyclones. Since such records are not available, the stochastic cyclone sampling approach has been used to develop information about the likelihood of more extreme storm tide levels. It should be noted however, that the synthetic cyclone sea levels do not include the effects of waves. While the effect of wave setup is relatively minimal at the tide gauge site due to its sheltered location, other more wave-exposed coastal locations may experience considerably higher water levels due to wave setup (see for example Hoeke et al, 2013a).

2.2.3 Wave Climate

Wave climate information is derived from the PACCSAP 30-year Wave Hindcast (Durrant, et al. 2013). This hindcast provides hourly gridded bulk wave statistics (e.g. significant wave height, peak wave period and peak wave direction) at 4 arcminute (~approx. 7 km) spatial resolution, including around the Samoa archipelago. It also provides hourly directional wave spectra at locations indicated by red x's in Fig. 6. Analysis of bulk wave statistics at the "SamoaN" and "SamoaS" spectral output point has been used to define the regional wave climate. Empirical return intervals (RIs) of large wave events (>99th percentile) were calculated by fitting a GPD using the maximum-likelihood method. Return periods of extreme waves at SamoaN are shown in Fig. 7. It is noteworthy that all historical wave events with greater than a 5 year return interval are associated with the passage of named tropical cyclones. Note that significant wave heights for Cyclone Evan (also shown for comparison) were slightly less than 5 years, indicating that waves associated with Evan were not extreme compared to other historical cyclones affecting Apia. Similar results as presented in Fig. 7 were found for SamoaS (not shown). This demonstrates that extreme wave events impacting Samoa are most likely generated by tropical cyclones. These large waves (> 5m significant wave height) are likely to have a substantial influence on local extreme sea levels.

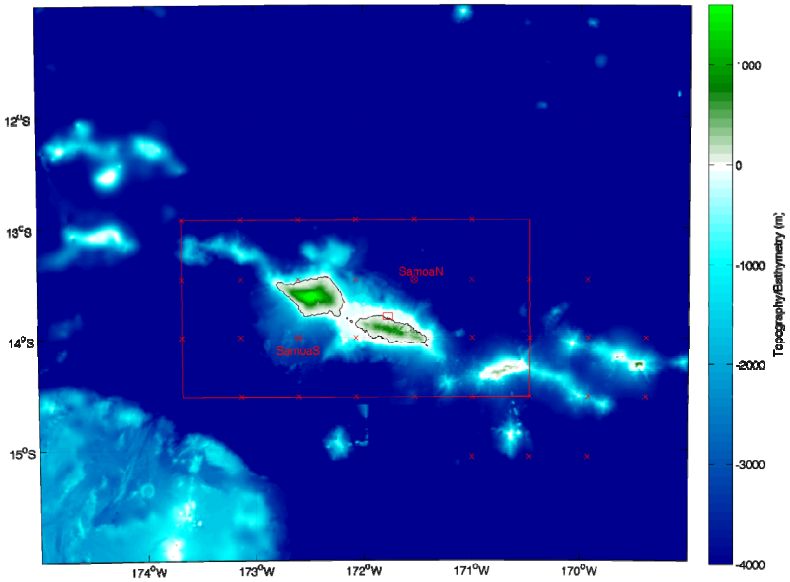

Fig. 6 Samoa storm surge and wave modelling grids: the entire plotted area is used for archipelago storm-surge model (GCOM2D) and wave model (SWAN) configuration used for synthetic cyclone cases; these areas are modelled at 1km and 5 km resolution respectively. The red-box around the islands of Upolu and Savai'i indicates a higher-resolution wave (SWAN) model (1 km resolution). This box is nested within the PACCSAP 30-year wave hindcast for historical runs and within the larger 5 km SWAN model for synthetic cyclone runs. PACCSAP 30-year wave hindcast spectral output points are plotted with red x's. The two red x's circled and labelled "SamoaN" and "SamoaS" are spectral output points used to define regional wave climate in the following sections. The small red box on the north shore of Upolu is the coupled wave-flow (Delft3D) model domain, centred on Apia, referred to as the 'Apia Model'.

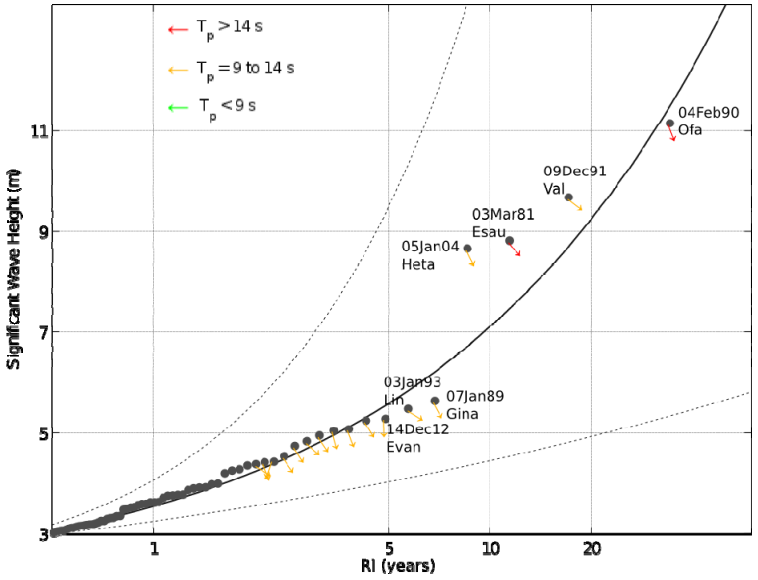

Fig. 7 Return intervals (RI) of significant wave height events>99th percentile values at SamoaN (see Fig. 6 for location). Peak wave direction is indicated with an arrow and peak wave period (T_p) with the colour of the arrow for wave heights>4m. Dates and associated tropical cyclone names for RIs greater than approximately 5 years are also indicated. Dotted lines indicate the 95% confidence intervals.

2.3 Methodology

As part of the PACCSAP program, a study was undertaken to estimate the return periods of tropical cyclone-induced storm tides for the Samoan archipelago. The approach taken in that study was to use a hydrodynamic model to simulate the sea levels arising from a population of 3000 synthetically-generated cyclones (e.g. McInnes, et al. 2014). Attributes of the cyclones, such as their intensities, track (i.e. speed and direction of movement and location of the track with respect to Samoa) were sampled from distributions of these characteristics developed from observed cyclones that have occurred over the broader Samoan region. An idealised cyclone model (Holland, 2008) was used to generate pressure and wind fields associated with the tracks. These were used to force a hydrodynamic model to estimate the sea levels. In addition, the cyclone tracks were randomly phased with tides so that storm tides were simulated. The resulting maximum sea levels were then processed to produce tropical cyclone storm tide levels. A more detailed description of the methodology is given in Appendix A.

Table 1 summarises the tropical cyclone storm tide heights estimated for a selection of return periods for Apia. These storm tide heights do not include wave-driven wave setup and wave run-up. Thus the estimated heights are more relevant for coastal locations that experience little or no additional increase in water levels due to wave breaking, such as those observed at the Apia tide gauge. It is important to note that, due to the relative rarity of tropical cyclones, at shorter return periods (50 years or less) the estimated levels are lower than those estimated directly from the tide gauge data and due to other combinations of more frequently occurring high tide and weather conditions, e.g. Fig. 5. However, it is also important to note that away from the sheltered tide gauge locations the inclusion of wave-breaking processes associated with the cyclone winds can produce coastal sea levels that are considerably higher than the levels presented here.

An estimation of the wave height return periods associated with the synthetic cyclones would require the running of a wave model for all synthetic cyclone events studied above. However, due to the high computational cost of regional spectral wave simulations, this was not possible in the time frame of this study. Rather, the approach taken was to select an ensemble of the ten synthetic cyclone events that produced storm tide water levels (i.e. tide plus surge) nearest (within ±0.03 m) to each of the return period heights in Table 1 from the entire synthetic cyclone population. Each of the ensembles' members were then used to simulate the sea level response with models that incorporated the combination of wind, pressure, tide and wave forcing at high spatial resolution. In this way, the contribution to the extreme water levels from wave breaking at the location of interest (i.e. Mulinu'u Peninsula) was estimated.

Table 1 Storm tide return periods estimated for Apia estimated from storm-tide modelling of a large population (3000) of synthetic tropical cyclones.

Return period	Storm tide Height (m)
100-yr	0.93
50-yr	0.80
20-yr	0.66

2.4 Climate Change Scenarios

Regional projections of mean sea-level rise for Samoa were obtained from Australian Bureau of Meteorology and CSIRO (2011). These projections include the effects of thermal expansion, the contribution to sea-level rise from ice sheets, glaciers and ice caps and the redistribution of mass in response to changes in ice sheets, terrestrial reservoirs and glaciers and ice caps, which alter the loading of the Earth and hence affect vertical crustal motion and the Earth's gravitational field. These effects lead to regional variations in the amount of sea level rise on climate timescales. Sea level changes for 2030 (2020–2039), 2055 (2046–2065) and 2090 (2080–2099), relative to 1990 (1980–1999), are available for a low, B1, medium, A1B and high A2 emission scenarios following the Special Report on Emissions Scenarios (SRES; Nakićenović et al., 2000) as indicated in Table 2. For this study we have elected to examine the impact of increased sea levels associated with the upper limit of the 95% range of the A1B scenario, with values of 0.14, 0.30 and 0.57m above the historical value for 2030, 2055 and 2090 respectively. The 95% values were selected in order to explore the impact of a broader range of future sea level rise scenarios that would be gained by selecting the midrange estimate. The selection of the upper estimate is also consistent with recent observational studies that report that sea levels are rising at a rate towards the upper end of the projected range of sea level rise (e.g. Rahmstorf et al, 2007). We note that these values do not differ from the upper range of the higher A2 scenario by more than 2 cm.

Table 2 Regional sea level rise projections (m) reproduced from PCCSP (2011) for Samoa. Values represent the multi-model mean change and the range in parenthesis is the 5–95% range.

Scenario	2030	2055	2090
B1	+0.10 (0.05–0.15)	+0.18 (0.10–0.26)	+0.31 (0.17–0.45)
A1B	+0.10 (0.06–0.14)	+0.21 (0.11–0.30)	+0.38 (0.20–0.57)
A2	+0.10 (0.05–0.15)	+0.20 (0.10–0.29)	+0.40 (0.21–0.59)

Under future climate conditions, it is possible that the behaviour of tropical cyclones may also change. In a tropical cyclone storm tide study for Fiji (McInnes et al., 2014) found that projected cyclone intensity and frequency changes had only a small effect on extreme sea-level heights for the 20-, 50- and 100-year return periods (See Appendix A). Such results are not yet available for Samoa but it is expected that the omission of these changes will not have a large effect on the results at the return periods that are being considered in this study.

The LiDAR data was provided relative to a 1973 mean sea level datum. However little documentation on how this datum was established is available and no tide gauge was deployed in Apia around 1973. This created uncertainty around using local datums to adjust background sea level to the baseline and future time periods; therefore water level

adjustments were performed using the global sea level reanalysis of Church and White (2011) to estimate mean sea level for a period centred on 1973 (1963-83) and finding differences with the baseline (1980-1999) period. To ensure that all modelled sea levels are relative to the 1973 datum as best as possible, this difference (increase 0.04 m) has been added to all sea level rise scenarios that are simulated.

3. NUMERICAL MODEL IMPLEMENTATION

To simulate the tide, surge and wave processes that contribute to extreme sea levels during severe storm conditions, a series of models have been implemented on different scales for modelling both historical as well as synthetic cyclone extreme water levels. Figure 6 shows the spatial coverage of the various models. Figure 8 describes the data flow between the models for the two main modelling configurations: historical and synthetic cyclone cases.

3.1 Samoa Archipelago Models

Three archipelago scale models have been used in this study. A hydrodynamic model, GCOM2D, was used to simulate the depth-averaged ocean currents and sea levels arising from tides, wind stress and atmospheric pressure (Hubert and McInnes, 1999). The other two models consist of the SWAN model (Booij, et al., 1999), a third generation spectral wave model, implemented over two regions at different spatial resolution. GCOM2D and the larger regional version of SWAN were run at 1 km and 5 km spatial resolution, respectively, for the area shown in Fig. 6. The SWAN model was also run at 1 km resolution for the area defined by the inner rectangle in Fig. 6. Additional information on the configuration of the SWAN model as implemented in this study is provided in Appendix B.

3.1.1 Bathymetry

Topographic and bathymetric data defining regions used by the GCOM2D and SWAN models was obtained from General Bathymetric Chart of the Oceans (GEBCO) data on a global 30 arc-second grid available at (www.gebco.net). These data use the 90 m Shuttle Radar Topography Mission data (available at srtm.csi.cgiar.org/) over land.

3.1.2 Tidal Forcing

Tidal heights on the lateral boundaries of the GCOM2D model are predicted using the tidal amplitudes and phases of the tidal constituents M2, N2, S2, K2, O1, K1, P1, Q1, Nu2, Ssa and Sa. The tide constituent data is obtained from the global tidal model of Le Provost et al., (1995).

3.1.3 Atmospheric Forcing

Meteorological forcing required by the GCOM2D and SWAN models consists of 10 m winds and mean sea level pressure (MSLP). Two sources are used in this study. For the purposes of running historical case studies, meteorological data is obtained from the National Centers for Environmental Prediction (NCEP) Climate Forecast System Reanalyses (CFSR) (Saha et al., 2010). The data is available globally at a horizontal resolution of ~38 km, and an hourly temporal resolution. The other source of winds and pressure for historical cyclones, as well as the synthetic cyclone cases, is the analytical cyclone model (Holland vortex) of Holland (2008), from which temporally and spatially varying wind and pressure fields are derived from cyclone track information. Generally, CFSR forcing was used for historical cases and Holland vortex for 'synthetic' cases. However, as discussed below, the Holland vortex was

also applied to selected historical cyclone tracks to allow inter-comparison between the same model using the two different sources of winds and MSLP.

For historical cases the 1 km SWAN model runs for the smaller geographical area use boundary input from the PACCSAP WW3 Hindcast, along with interpolated winds from the GCOM2D model. For synthetic cyclone cases, wave-boundary input to the 1 km SWAN model is generated by the larger extent 5km SWAN model, using interpolated winds from GCOM2D model as input.

3.2 Apia Model

For the simulation of coastal sea levels and currents around Apia, the Delft3D hydrodynamic modelling system was used (Lesser et al. 2004; Roelvink and Banning 1994). Although this modelling system was developed for use on low-slope sedimentary coastlines, it has been applied with some success to steeper erosional coasts (e.g., Hoeke et al. 2013b; Lowe et al. 2009; Mulligan et al. 2008). This system consists of a hydrodynamic module, hereafter referred to as the 'flow' module, and a wave module. The latter is provided by the SWAN model.

The flow module was set up on a 2D curvilinear grid, which varied in spatial resolution from approximately 200m near the northwest and southeast (lateral) boundaries, to approximately 10m near the Mulinu'u Peninsula and Apia Harbor. The grid boundaries are shown in Fig. 9, while examples of the grid cell boundaries near the centre of the grid are shown in Fig. 1.

The wave module simulations were performed on the same grid as the flow module, except the wave grid extended a further 5 grid points in the lateral and 2 grid points in the offshore directions. This was to minimize spurious fluctuations in the flow module due to sudden transitions in wave fields imposed at the wave boundaries.

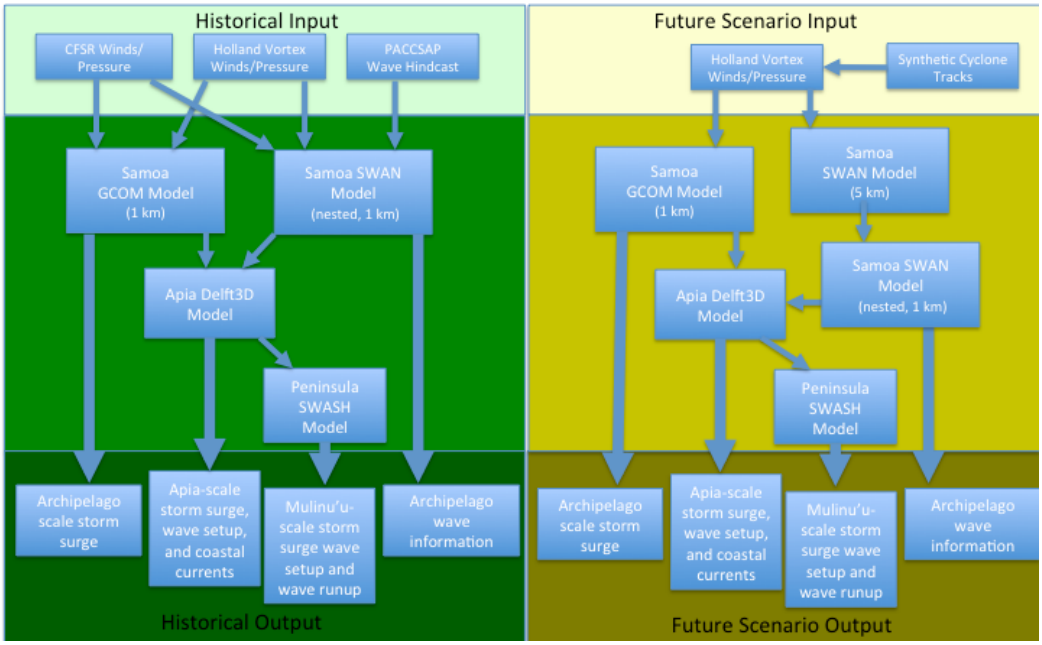

Fig. 8 The relationship of the various models, and their inputs and outputs that are used in the present study. The left hand panel shows the typical arrangement for running historical cyclone cases with meteorological data coming from either CFSR or Holland (2008). The right hand panel shows the configuration for synthetic cyclone cases for which only the Holland (2008) model is used to provide winds and pressure.

The two modules are iteratively coupled. This allows forces arising from total wave dissipation, calculated in the wave module, to be incorporated as additional surface stresses in the flow module, in order to compute wave-induced residual flow and Stokes drift. The subsequent water levels and currents in the circulation module are in turn passed back to the wave module for use in calculating an updated wave field. These interactions between the modules continue in turn.

Figure 9 also shows the locations of output points in the Apia Model, as discussed in the following section. In particular, in discussions and statistical values used for the Mulinu'u Peninsula, the locations T1.10, T2.7 and T1.12, T2.9 are used as representative locations for "in front of the sea wall" and for "behind the seawall".

3.2.1 Bathymetry

Bathymetric elevations in the coupled wave/flow Apia Model were specified using the recently acquired LiDAR data (Pelydryn, 2012). This data set provided nearly continuous topography and bathymetry of the coastal area of Apia at nominal spatial resolutions of about 1m and 3m and vertical accuracy of around 0.10 m and 0.55 m, respectively. Bathymetry in deeper areas (< 20 m) was supplemented by multi-beam data supplied by SPC-SOPAC and by GEBCO data (www.gebco.net). The LiDAR data provided crucial bottom boundary layer information to the Apia and Peninsula model, particularly on shallow reef morphology, which largely controls local wave setup processes (e.g. Buckley and Lowe, 2013; Hoeke et al., 2013b).

3.2.2 External Boundary Conditions

The offshore water level boundary was forced by either (1) tidal prediction + sea-level anomaly + inverse barometer effect (IBE); or (2) by output from the GCOM2D model at offshore boundary points. In the first case, used for historical runs only, the sea-level anomaly was provided by either low-pass filtered monthly sea-level values from tide gauge data (when available) or the CSIRO sea-level reconstruction (Church et al. 2011) and IBE calculated from CFSR surface atmospheric pressure. Correlations between either low-pass filtered monthly sea-level values and CSIRO sea-level reconstruction (Church et al. 2011) and IBE were greater than 0.90. All offshore water level boundaries whether historical or synthetic cyclone cases, were adjusted to be relative to the 1973 MSL datum.

The wave boundary conditions were provided by spectra from the SWAN 1 km model (see above discussion on the Apia Model), given at five segments on the offshore boundary. The wave module's set up was the same as for the SWAN models as also discussed above, and in Appendix B. Additional details on the Apia Model setup can be found in Appendix C.

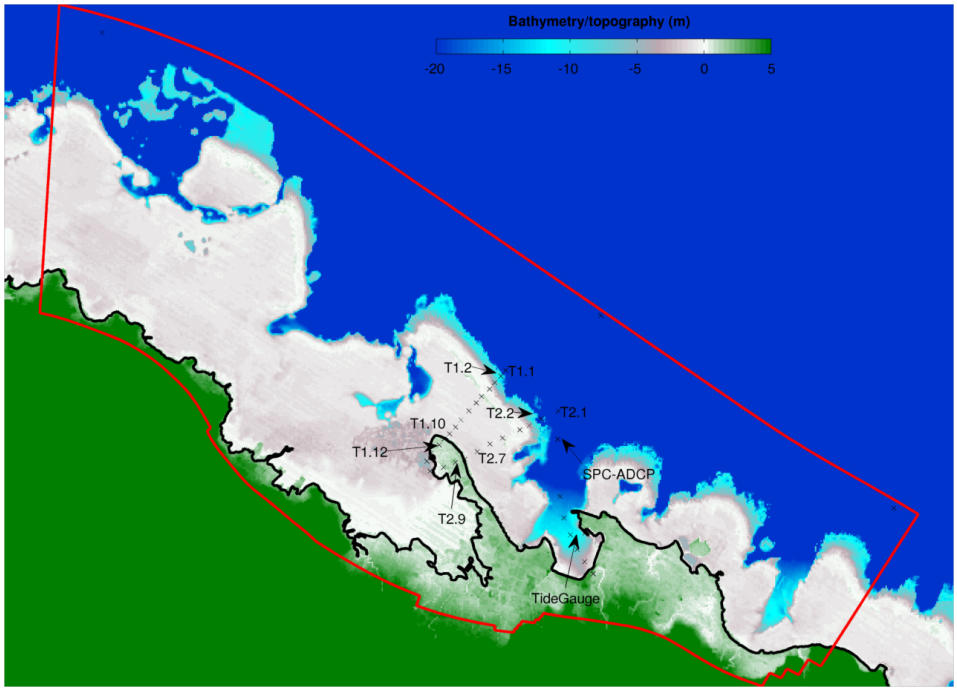

Fig. 9 The region covered by the Apia Model. The model grid, the boundaries of which are indicated by red lines, is a curvilinear grid. The resolution varies from approximately 200m near the northwest and southeast (lateral) boundaries, to approximately 10m near the Mulinu'u Peninsula and Apia Harbor. Boundary conditions for waves, currents and sea-level heights from the archipelago models are determined for the three locations indicated by black x's on the outer boundary, and subsequently interpolated to the boundary grid points of the Apia Model. Detailed model output is generated at the points in the interior of the grid, indicated by black x's. Points with text labels are discussed in the text.

3.3 Peninsula Model

The Apia Scale models described in the previous section provide simulations of spectral wave conditions and hydrodynamic circulation, including wetting and drying of land areas due to tides, waves and storm surge. However, the Apia Model's wave module (SWAN) is a phase-averaged model. Therefore it does not resolve individual waves and is thus unable to directly simulate the propagation and dissipation (breaking) of individual waves, the generation of infragravity waves, individual wave run-up, and potential overtopping of coastal structures such as seawalls. These phenomena are estimated using a non-hydrostatic wave-flow model which predicts the transformation of surface waves due to nonlinear wave-wave interactions, interaction of waves with currents, and wave breaking and run-up at the shoreline. The model selected for this task is the Simulating Waves till Shore (SWASH) model as it tends to provide a more robust and faster solution than a (similarly wave-phase resolving) Boussinesq solution (Zijlema et al., 2011; Zijlema, 2012). This model was set up in a 1-dimensional, 0.5 m resolution mode, along a 2 km transect extending beyond the reef edge from the northeast side of Mulinu'u Peninsula (see Fig. 9 for location of the output transect T1 to T2).

3.3.1 Bathymetry

In addition to incident wave and water level conditions, wave shoaling is also sensitive to water depth and bottom roughness. The LiDAR elevation data was used to create an idealized elevation profile at 1 m resolution (see Appendix D for details).

The seawall was not adequately resolved in the regridded LiDAR dataset and so was manually inserted into the profile based on the design parameters of the leading slope, crest height and crest width (JICA, 1993). These profiles were then used to test the sensitivity of wave propagation in the Peninsula Model to water depth (Table 3).

3.3.2 Parameter Settings

In the absence of observational measurements in the vicinity of Mulinu'u Peninsula with which to calibrate the Peninsula Model, the approach taken in this study has been to select parameter values that span the range of plausible values under similar reef settings, as presented in the scientific literature (Vetter et al., 2012; Buckley and Lowe, 2013). To constrain the number of model simulations needed to sample the range of results obtained by using different combinations of parameter settings, the parameter values have been grouped to provide a 'best case' (minimal inundation) scenario, a 'worst case' (maximal inundation) scenario and a mid-range or 'optimal parameterization' scenario (Table 3). The key results section reports on runs using the 'optimal parameterization' settings, while the uncertainty range in the presentation of results is provided by the range of H_s and peak wave period (T_p) values as determined from the Apia Model simulations for each 10-member ensemble of runs. More details of the parameter settings used in the Peninsula Model are described in Appendix D.

Table 3 Summary of parameters used in the SWASH model grouped according to their influence on degree of inundation.

Variable	Optimal Parameters	High Sensitivity (Large inundation)	Low Sensitivity (Small inundation)
Profile	Mean depth profile	Lowest profile (deepest water)	Highest profile (shallowest water)
Friction (Manning's coefficient)	0.04 (USGS, boulders)	0.03 (USGS, cobble)	0.04 (USGS, boulders)
Breaking parameter (α)	0.9	0.8	1.0
Seawall height	2.4 (LiDAR)	2.4 (LiDAR)	2.6 (JICA, 1993)
Seawall leading slope	1:1.7 (LiDAR)	1:1.7 (LiDAR)	1:1.5 (JICA, 1993)

In carrying out the simulations, the model is run for 45 minutes, allowing for model spin-up over the first 30 minutes. Results are extracted from the final 15 minutes of the simulation. The wave setup is computed from the 50th percentile of the 1-second output water levels, while wave run-up is determined from the 98th percentile water levels. Velocity magnitudes are also analysed to determine the 50th and 98th percentile values.

3.4 Synthetic Cyclone Selection for Wave and Surge Joint Probability

This section describes the approach and rationale for estimating the sea-level extremes, and relevant wave and current parameters using the models described in the previous section.

From the synthetic storm tide simulation database, 30 tropical cyclone/storm tide events were selected, 10 events each for return periods of 20, 50 and 100 years. These events were selected based on maximum simulated storm tide near the Apia tide gauge from the Archipelago GCOM2D model that were within ±0.03 m of each respective return period value (Table 1) at the approximate location of the seaward boundary of the Apia Model domain (i.e. sufficiently offshore to not be affected by wave setup). Although an ensemble of greater than 10 cyclone events for each return period would be desirable, it was not possible within the time constraints of the present study to model a larger selection of events. The tracks of the 30 selected synthetic cyclones cases are shown in Fig. 10, while the various cyclone parameters associated with these particular cyclones are provided in Table 4.

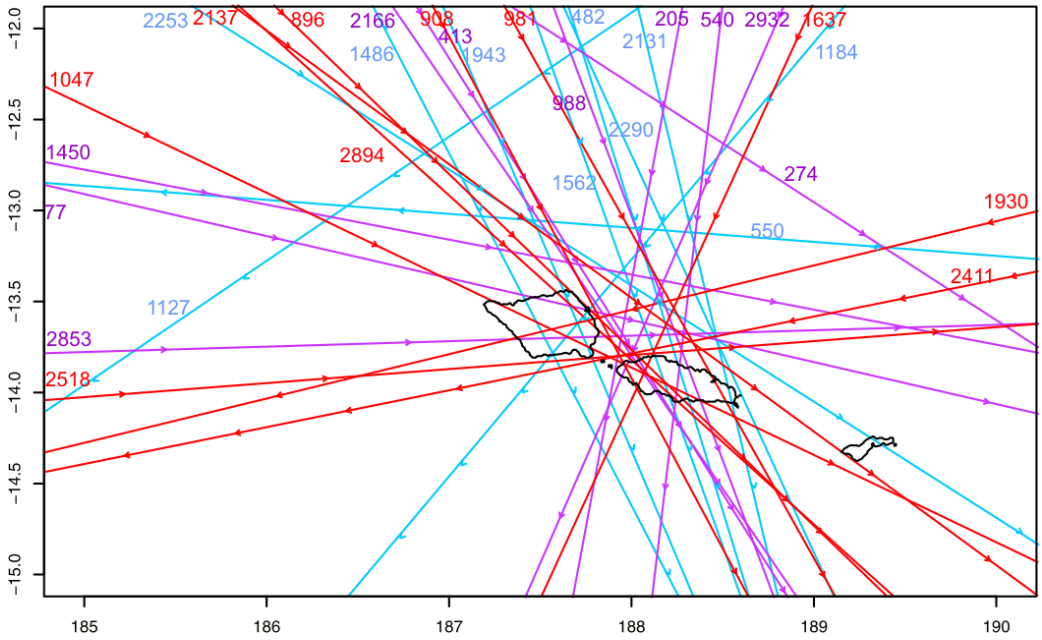

Fig. 10 The synthetic cyclone track numbers selected to represent the 1-in-20, 1-in-50 and 1-in-100 year storm tide events (blue, purple and red, respectively) from the synthetic cyclone database. Cyclone track information for these cyclones is given in Appendix E.

The selected ensemble events were re-simulated in the Archipelago GCOM2D model and simulated in the Archipelago SWAN model in order to store the water levels, currents and waves fields at 30-minute intervals to provide relevant forcing conditions for the Apia Model. Thus, the Samoan Archipelago models provided tide, wind, storm surge and wave forcing along the Apia Model's boundary at 30-min intervals for the synthetic cyclone ensemble members (as schematized in Fig. 8). The maximum wave and sea-level values calculated by the Apia Model for each ensemble event were then used to provide a central estimate and range of possible wave values and sea-level for each set of ensembles to the Peninsula Model.

Table 4 Summary of synthetic cyclone parameters used in the SWAN and Apia Harbour modelling. The last two columns are radius of maximum winds (RMW) and maximum storm-tide water level (η), respectively.

Run #	Date (yyyymmdd)	Time (hr)	Pressure (hPa)	Long. (deg)	Lat (deg).	Direc (Deg from N)	Speed (km/hr)	RMW (km)	η (m)
20-yr									
2253	19920102	0	933	188.2	-13.6	123	19	24.4	0.65
482	19840209	2200	970	188	-13.2	163	25	30.9	0.68
550	19861230	2000	975	187.8	-13.2	275	22.2	32	0.66
1127	19880315	2200	951	187.3	-12.5	235	16.1	26.7	0.70
1486	19900326	2000	948	187.8	-14.2	153	17.9	27.4	0.71
2131	19930207	1800	949	188.5	-14.1	167	21	27.5	0.65
1184	19780306	2200	942	187.2	-14.2	219	9	26.3	0.65
1562	19881220	1800	978	188.2	-14	161	13.7	33.4	0.68
2290	19841122	500	945	188.7	-14.4	156	37.8	26.9	0.67
1943	19800317	2100	962	187.7	-13.8	158	14.1	29.8	0.66
50-yr									
2932	19760105	0	946	188.6	-12.4	203	15.8	25.7	0.79
274	19940225	700	971	189.3	-14.6	134	11.1	32.3	0.82
77	19770112	1000	947	188.6	-13.8	103	30.1	26.9	0.82
988	19790221	700	974	188.4	-14.3	160	14.1	32.8	0.80
2166	19770121	2300	961	188.7	-14.9	146	25.7	30.4	0.82
2853	19910220	200	945	187	-13.7	88	21.9	26.5	0.81
1450	19801221	1200	965	189.5	-13.7	101	22.9	30.3	0.83
540	19931201	1400	956	188.1	-13.2	190	20.6	28.2	0.78
205	19931112	0	915	188.1	-12.7	190	19.4	21	0.79
413	19780406	2000	979	188.2	-14.1	148	9.2	33.7	0.77
100-yr									
896	19940112	2200	951	188.5	-14.3	134	10.4	28	0.92
1930	19820223	2000	935	187.5	-13.7	256	32.4	24.8	0.92
1047	19870112	800	920	188.6	-14.2	116	22.3	22.7	0.91
2137	19930127	1300	950	187.5	-13.2	126	13.7	27	0.94
2411	19781230	1900	983	187	-14.1	258	10.5	34.6	0.91
2518	19870207	300	944	188.9	-13.8	86	18.1	26.4	0.95
2894	19870218	2000	955	187.8	-13.7	132	28.3	28.3	0.96
981	19831017	1900	944	188.8	-14.5	152	17.5	26.9	0.94
908	19880215	300	959	187.9	-13.9	152	19.1	29.3	0.90
1637	19850214	1900	976	188.6	-12.7	204	18.1	31.8	0.88

4. MODEL VALIDATION

In this section, output of the models is compared to historical events.

4.1.1 Archipelago Wave Models

Although no known *in situ* wave data exists in the Samoan region during tropical cyclones with which to compare with the archipelago SWAN (or Apia) model, the PACCSAP Wave Watch III (WW3) model has been well validated with *in situ* wave buoys in other areas of the Pacific, as well as by using global satellite altimetry observations. The latter data are too sparse in space and time to validate a single tropical cyclone event, however. Therefore, to test the ability of the Samoa Archipelago SWAN model to simulate realistic wave conditions, several simulations of historical tropical cyclones were performed using several combinations of the atmospheric and wave forcing types outlined in Section 3. The results were compared with each other and with WW3 data. Examples of the comparisons are shown in Fig. 11.

The forcing types include:

1. SWAN nest (CFSR): the SWAN nest boundaries (see Fig. 6) are forced with WW3 spectra, with CFSR winds over the nest area. This is standard for historical events.
2. SWAN CFSR: the entire grid domain (5km resolution SWAN and 1km nest) is forced with CFSR winds, with no external boundary forcing. This is the same as for the synthetic cyclone cases, except with historical CFSR winds.
3. SWAN Holland vortex: uses the same as SWAN CFSR, but with a wind field generated by a Holland vortex, based on the characteristics of the historical cyclones, e.g. the same as the synthetic cyclone cases, but with a historical storm track.

At the deepwater locations, SamoaN and SamoaS (Fig. 6), generally excellent agreement was found between WW3 and SWAN with CFSR forcing: deepwater bulk wave characteristics were virtually indistinguishable between WW3 and SWAN CFSR nest, although SWAN CFSR tended to estimate slightly larger significant wave heights (H_s) around the peak. Without *in situ* observations it is difficult to ascertain whether this is due to the choice of the wind source term within SWAN (Komen et al. 1984); or because SWAN does not dissipate deepwater swell energy (this is generally only significant at ocean basin scales); or that the coarser spatial resolution WW3 model may actually slightly underestimate peak wave heights in tropical cyclone conditions. Differences in wave characteristic between WW3 and SWAN Holland are greater; this is to be expected since the Holland vortex model cannot account for all variations in real tropical cyclone wind fields. However, the differences are not systematic and peaks in wave energy tended to occur at the same time; this is further supported by the finding that just offshore from Apia, the maximum wave heights and periods of historical tropical cyclones (using SWAN nest type forcing) fell within the mid to low range of that of the synthetic cyclone runs (e.g. see Fig. 14 in the results section). Thus, there is high confidence that the archipelago SWAN model produces climatologically realistic wave characteristics near the peak in wave heights when using synthetic tropical cyclone forcing.

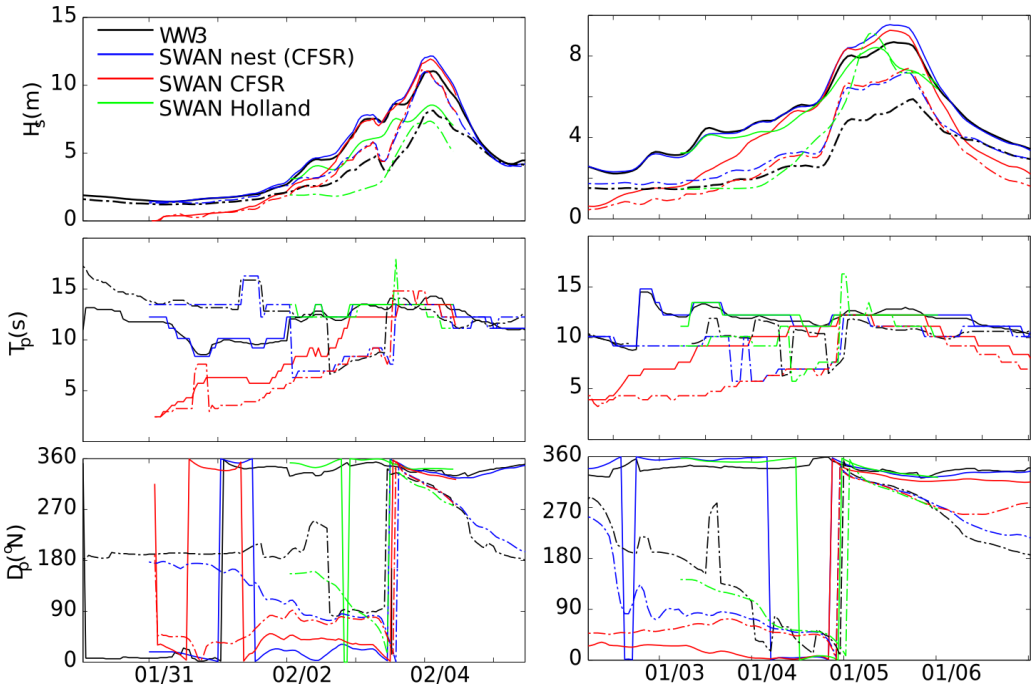

Fig. 11 Comparison of the PACCSAP Wave Watch III Hindcast (WW3, black lines) and the Samoa SWAN models (Fig. 7) at two internal points ('SamoaN' and 'SamoaS' in Fig. 6, solid and dashed lines respectively) during Cyclones Ofa (left panels) and Heta (right panels). Variables plotted include significant wave heights (H_s), peak period (T_p) and peak wave direction (D_p) in the top, middle and bottom panels respectively. Three different types of forcing for the Samoa SWAN models are considered: one with spectral wave boundary input and CFSR wind forcing of the 1 km SWAN 'nest' grid only (blue lines, used for historical cases); no wave boundary input, but using CFSR winds across the entire 5 km and 1 km nested SWAN grids (red lines, run on the grid configuration for synthetic cyclone cases but with historical winds); and Holland vortex winds across the entire 5 km and 1 km nested SWAN grids (green lines, the type of forcing used for all synthetic runs. Solid lines represent 'SamoaN', dashed lines 'SamoaS'.

4.1.2 Apia Model

A pressure sensor on an acoustic Doppler current profiler (ADCP) deployed by the Secretariat of the Pacific Community's Applied Geoscience and Technology Division (SPC-SOPAC) between February 3 and 24, 2004 provided additional *in situ* observations of coastal water levels near Apia. While no tropical cyclones were in the vicinity during this time period, Apia Model simulations were performed for this time period so as to compare modelled and observed water levels at two location: the ADCP and the tide gauge. Correlation coefficients between water levels simulated by the Apia Model and those observed by the ADCP and the tide gauge for this period were 0.992 and 0.998, respectively (Fig. 12) and root-mean-square errors were 0.04 m and 0.03 m, respectively, indicating excellent agreement. Correlation between the tide gauge and model simulations during historical tropical cyclone events for which there is data (Heta and Tui) are slightly lower, 0.963 and 0.985, respectively. The difference between simulated and observed water level residuals at the tide gauge near the peak for Heta and Tui is at most 7 cm, and usually better. An example of simulated and observed tide gauge water levels during Cyclone Heta is presented in Fig. 13. Although this

indicates high model skill for the estimation of water levels at the tide gauge, inspection of model output during peak water levels (e.g. Fig. ES3) shows that water levels may be 1 metre or more higher over the surrounding reef flats compared to at the tide gauge location. This is primarily due to wave setup. Because of the lack of *in situ* observations of water levels over the reef flats, the values of bottom boundary layer (bed) roughness coefficients (see appendix for description) could not be calibrated. As previously mentioned, LiDAR bathymetry cannot be used to directly estimate bed-roughness over coral reefs as its resolution is too coarse and because of dependence on hydrodynamic length scales, requiring calibration through hydrodynamic observations (Jaramillo and Pawlak, 2011).

Several studies have noted the sensitivity of hydrodynamics of coral reefs to these coefficients (Buckley and Lowe, 2013; Hoeke et al., 2013b). In order to assess the nature of this sensitivity, a series of simulations were performed for a selected number of historical and synthetic cases. Bed roughness was varied from one half to double (i.e. a factor of two) across the central values used in the main results of this study. The differences in circulation and water levels produced by these changes in bed roughness were often complex, as hydrodynamic structures sometimes changed (e.g. locations of rip currents). However, differences in maximum water levels near the Mulinu'u Peninsula and other back reef areas were generally between ±1% and ±3%, with the slightly lower water levels near the reef edge and slightly higher water levels near to shore with decreasing bed roughness. The difference in maximum current areas was greater, ±5% and ±25%, particularly near the tip of the Mulinu'u Peninsula. Generally, maximum current velocities increased with decreasing roughness values, and vice-versa.

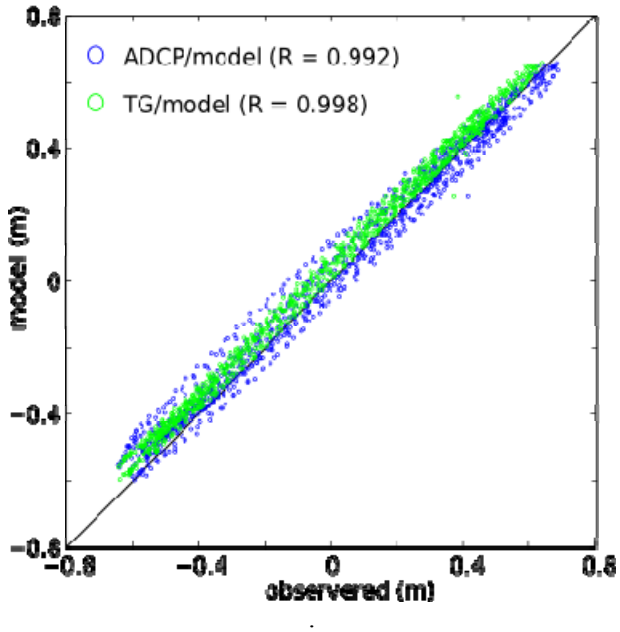

Fig. 12 Quantile/quantile plot of observed (x-axis) and simulated (y-axis) values of water level at the ADCP and the Apia Tide Gauge from February 3 and 24, 2004. Correlation coefficients (R) are given in the upper left hand corner.

The lack of *in situ* observations over the reef flats surrounding the Apia Harbour and Mulinu'u Peninsula is arguably the single largest source of uncertainty in assessing the models' ability to realistically simulate hydrodynamics. Without such observations parameters controlling wave setup, wind setup and wave dissipation (e.g. nearshore wave heights) are difficult to calibrate and a thoroughly quantitative assessment of model skill at simulating these processes is not possible. The central values for bed roughness listed in the appendix are used in all results presented in this study. These values were used due to the level of qualitative agreement between the Apia historical simulations and reports of damage and inundation during historical cyclones, especially Ofa (Rearic, 1990).

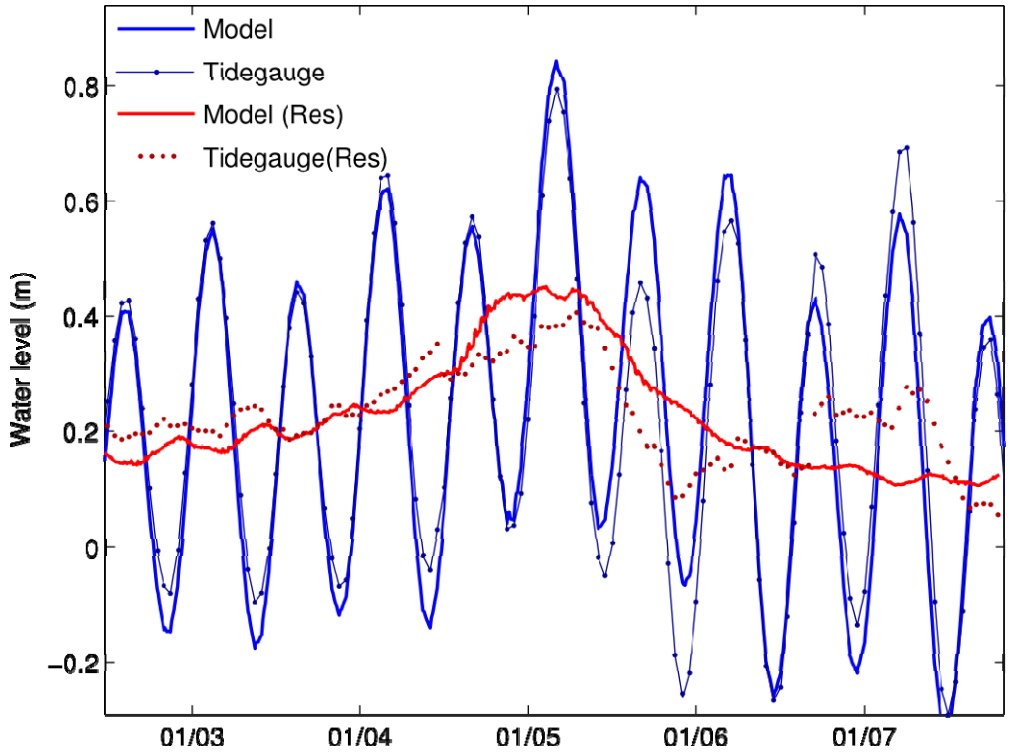

Fig. 13 Modelled and observed water levels (blue) and residuals (red) during Cyclone Heta.

4.1.3 Peninsula Model

As with the Apia Model, the lack of *in situ* observations across the reef fronting the Mulinu'u Peninsula introduces a high degree of uncertainty into parameter selection for the model. As a result of this, and also the difficulty in qualitative comparison between the Peninsula Model and historical events, an estimate of the full range of plausible parameter values for the Peninsula Model is presented in the results.

5. RESULTS

5.1 Archipelago Wave Model Results

The maximum significant wave height ($H_s$max) modelled in each of the thirty simulations (Table 4) is shown in Fig. 14 for a location on the boundary of the Apia Model domain. For comparison, $H_s$max at the reef slope fronting the Mulinu'u Peninsula (T1.2 and T2.2 in Fig. 9) from the Apia Model (used to define input to the Peninsula Model) is also shown. These results show that, within each ensemble of runs for the 20-year, 50-year and 100-year storms, there is a large spread in wave height simulations. This is about 6 - 20 m at the offshore boundary, and between 5 – 14 m at the reef slope. The varying decrease in $H_s$max between the offshore boundary and the nearshore reef slope is related to the (sometimes) oblique angle of wave approach to the reef and the presence of deeper (30-50m) reefs offshore. The sensitivity of offshore/nearshore wave heights on angle of wave approach is caused by two processes: directional spreading/refraction and wave dissipation due to bottom friction between the offshore boundary and the 'toe' of the reef slope (around T1.1 and T2.1).

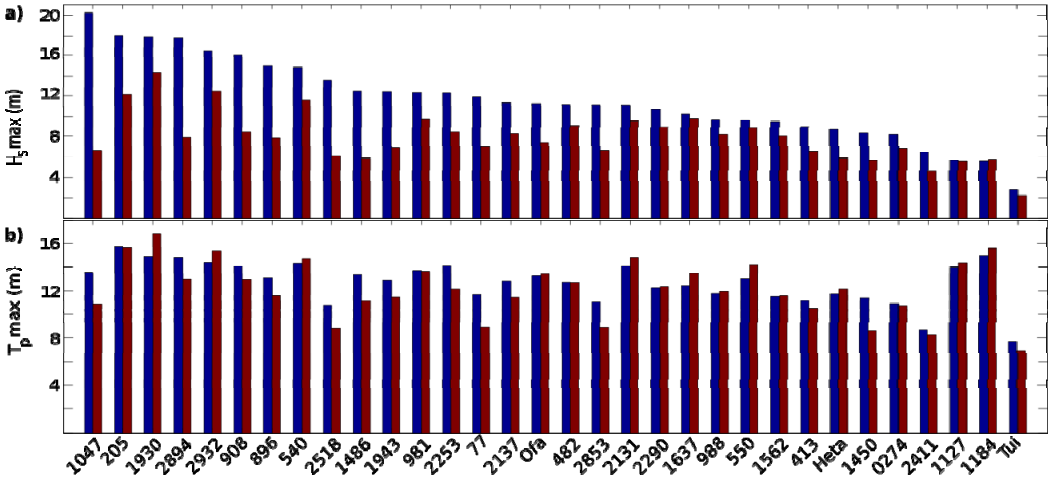

Fig. 14 (a) Maximum significant wave height ($H_s$max, upper plot) and (b) maximum peak wave period ($T_p$max, lower plot) of the synthetic cyclone events listed in Table 4 as well as historical cyclones (Ofa, Heta and Tui). Blue bars values at the offshore boundary of the Apia Model. Red bars indicate the mean $H_s$max and $T_p$max at the Apia Model locations T1.2 and T2.2, used to define the range of wave input to the Peninsula Model.

Also shown are the maximum peak wave periods ($T_p$max) for each of the simulations; these range from about 10-17 s. Both $H_s$max and $T_p$max show dependence on the characteristics of the synthetic cyclones, such as intensity, speed of movement and track. The two largest events were from tracks that approached Apia from the north, while the weakest events were associated with weaker cyclones. The $H_s$max values for the historical cyclones Ofa, Heta and Tui are also shown in Fig. 14. They fall within the mid to low range of the synthetic cyclone wave fields at Apia.

The simulated wind and wave fields for two synthetic tropical cyclones cases at around the time of $H_s$max are shown in Fig. 15. Event 981, which approached from the northwest, produced $H_s$max of about 11 m at Apia (Fig. 15 a, b). The second example is event 2411. It approached from the northeast, with the maximum wind field to the south of Apia resulting in lower $H_s$max values of around 5 m (Figs 15 c , d).

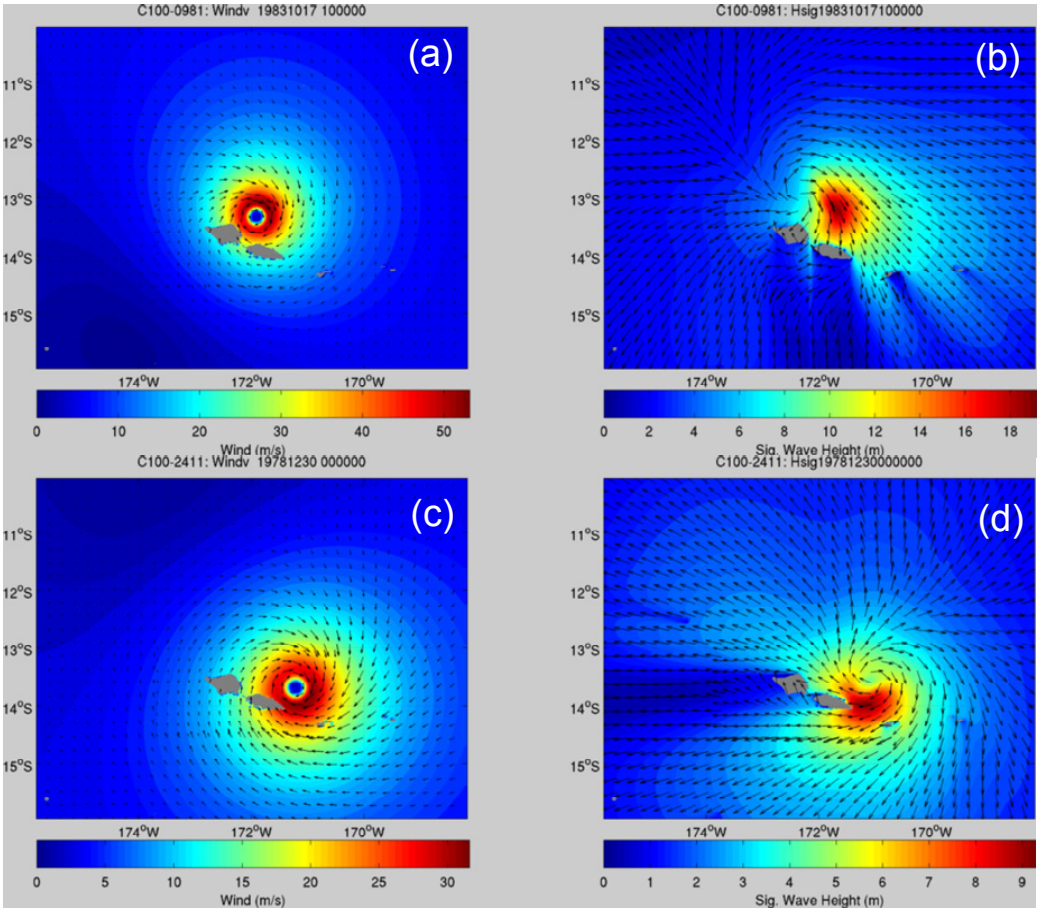

Fig. 15 The Holland wind field and SWAN modelled wave field of two synthetic cyclone events close to the time of maximum wave heights ($H_s$max) at Apia. (a) Wind field of synthetic cyclone #981 that approached Apia from the northwest (b) the associated modelled significant wave height (H_s) (c) wind field of synthetic cyclone #2411 that approached Apia from the northeast and (d) the associated H_s.

5.2 Apia Model Results

Archipelago wave and storm tide simulations provided forcing for the Apia Model for baseline (1990) sea level conditions and also three future sea level scenarios. Thus a total of 120 coupled wave-flow Apia simulations using synthetic forcing were conducted. The median significant wave (H_s) fields for the ensemble of 20-year and 100-year cyclone events under 1990 and 2090 sea levels are shown in Fig. 16. These are qualitatively similar to historical results (e.g. Fig. ES3): significant dissipation of wave energy occurs at the reef edge; across the neashore side of the reef flats, values of H_s are typically less than 1-3 m, although significant wave penetration into Apia Harbor is evident. Median values of H_s from the 1-in-

100 year storm tide events are higher than those for the 1-in-20 year events, which is consistent with the fact that in general, the more intense cyclones associated with higher storm tides will also tend to produce larger waves. However, for an individual event, this relationship does not necessarily hold, as shown by the results in Fig. 14a, as wave height depends not only on wind speed, but also cyclone track and forward speed. Comparing Figs 16a with 16c and 16b with 16d, it can be seen that higher mean sea level conditions lead to only minor increases in H_s nearshore.

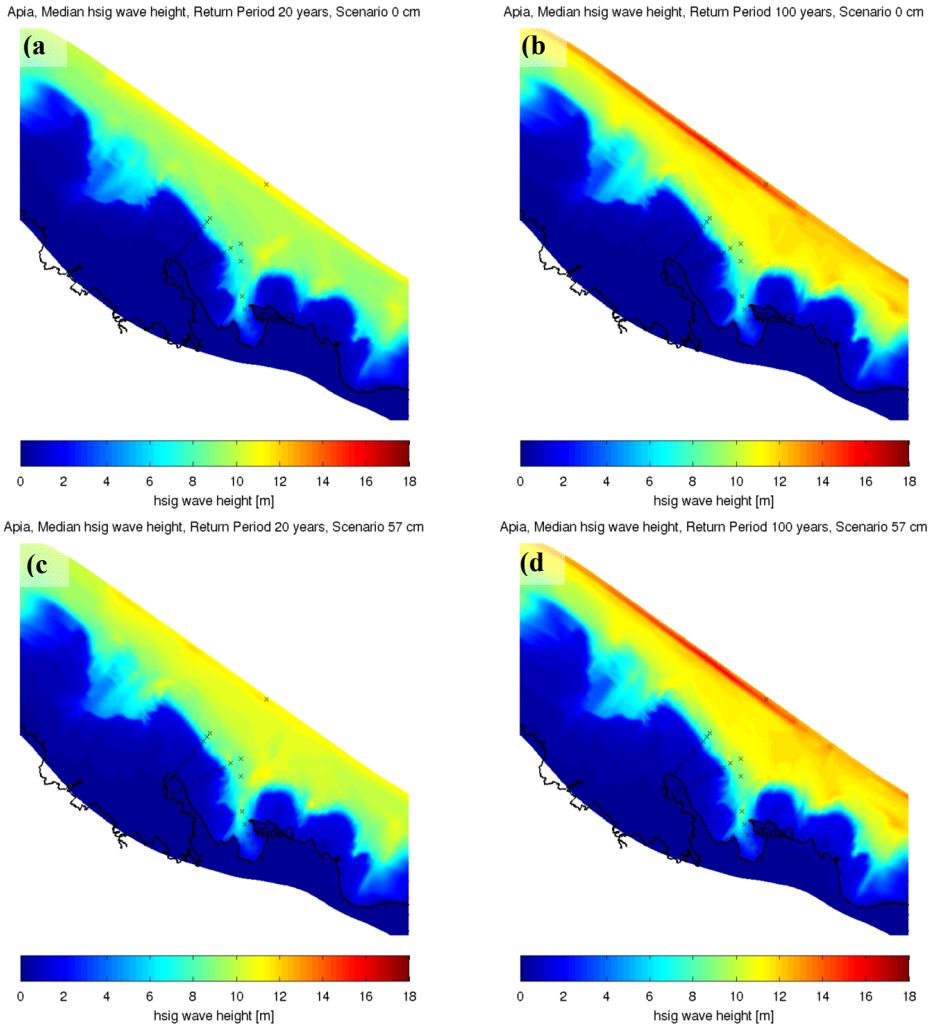

Fig. 16 Median value of the significant wave height for (a) the 1-in-20 and (b) the 1-in-100 year simulations under baseline (1990) sea level conditions and (c) the 1-in-20 and (d) the 1-in-100 year simulations under 2090 sea level conditions. Wave heights are relative to 1973 MSL.

As with the wave results, the maximum water levels attained throughout each of the 120 Apia simulations were used to determine a median value estimated for each ensemble. Median values for the 20-, 50- and 100-year ensembles under the four sea-level conditions are shown in Figs. 17-19.

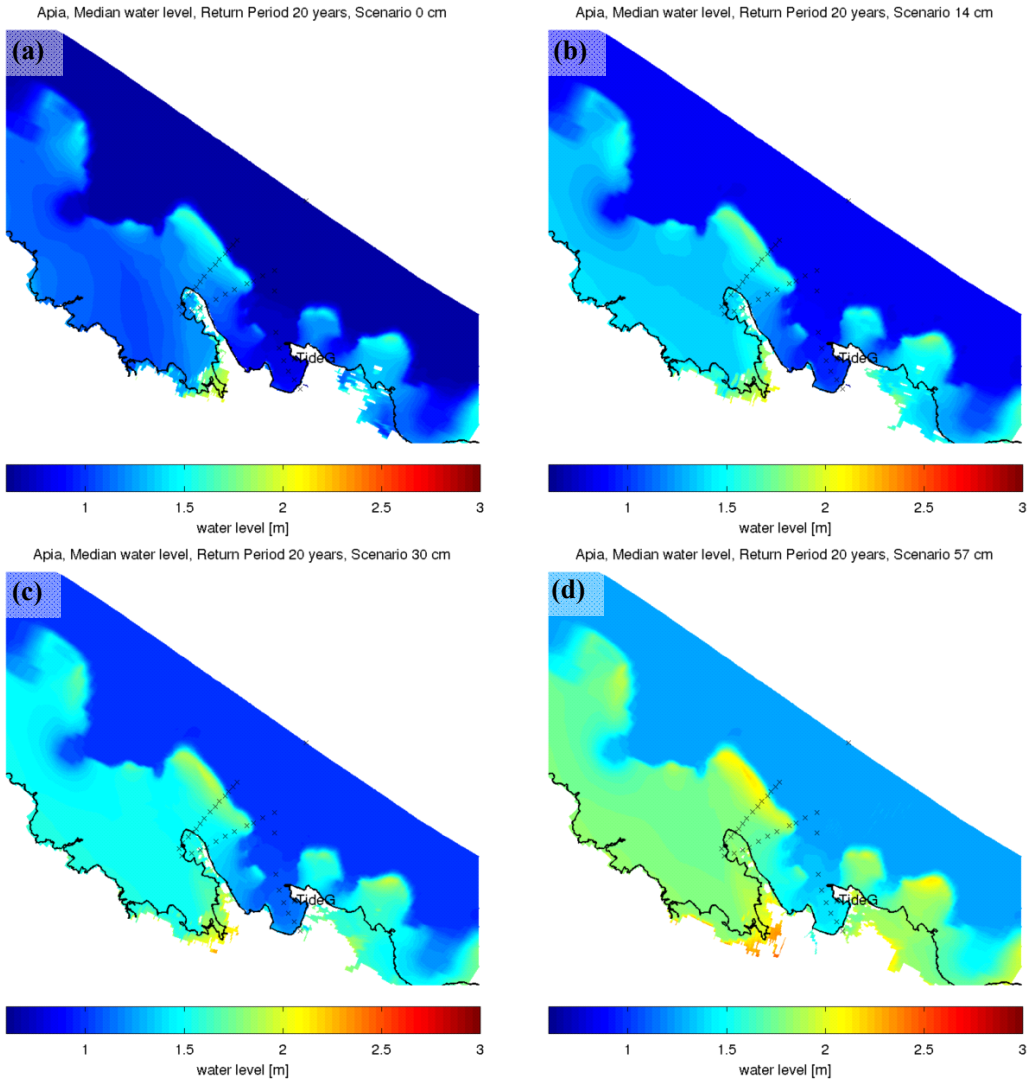

Fig. 17 Median value of the maximum modelled storm tide height (including wave setup) for the 1-in-20 year events under (a) baseline (1990), (b) 2030, (c) 2055 and (d) 2090 sea level conditions. Sea level heights are relative to 1973 MSL.

These figures show that in general, in the deeper water, sea levels are little changed from the values imposed from the larger scale GCOM2D simulations. However, in the shallower water between the reef edges and the coast, maximum sea levels occur. This is mostly due to wave setup, leading to a pattern of sea-level response that is roughly opposite to that of wave height (Fig. 16), i.e. where wave height most quickly decreases, mean water level most quickly increases according to the well-known wave radiation stress gradient relationship. It is worth noting that, at the location of the tide gauge, sea levels are elevated only slightly higher than the deep water locations close to the offshore boundary. This indicates that often tide gauges do not sample the extreme sea levels than occur as a result of wave breaking processes (e.g. wave setup). This is due to their generally sheltered situations (Hoeke et al, 2013a). The small degree of increase in sea levels in the harbour is likely to be mostly due to wind setup. A much greater amount of wind setup is evident within Vaiusu Bay to the west of Mulinu'u Peninsula, often resulting in significant levels of inundation of the Peninsula from the western

side. Along the ocean-facing coastline to the east of the tide gauge location, the inundation extent in general increases with increasing sea level rise, as expected.

For 2055 and 2090 sea-level rise scenarios, the entire northern end of Mulinu'u Peninsula becomes inundated under water level conditions associated with 20-year and 50-year tropical cyclone storm tides (Figs 17 and 18). For a 100-year tropical cyclone storm tide (Fig. 19) extensive inundation of the peninsula is apparent under present sea-level conditions.

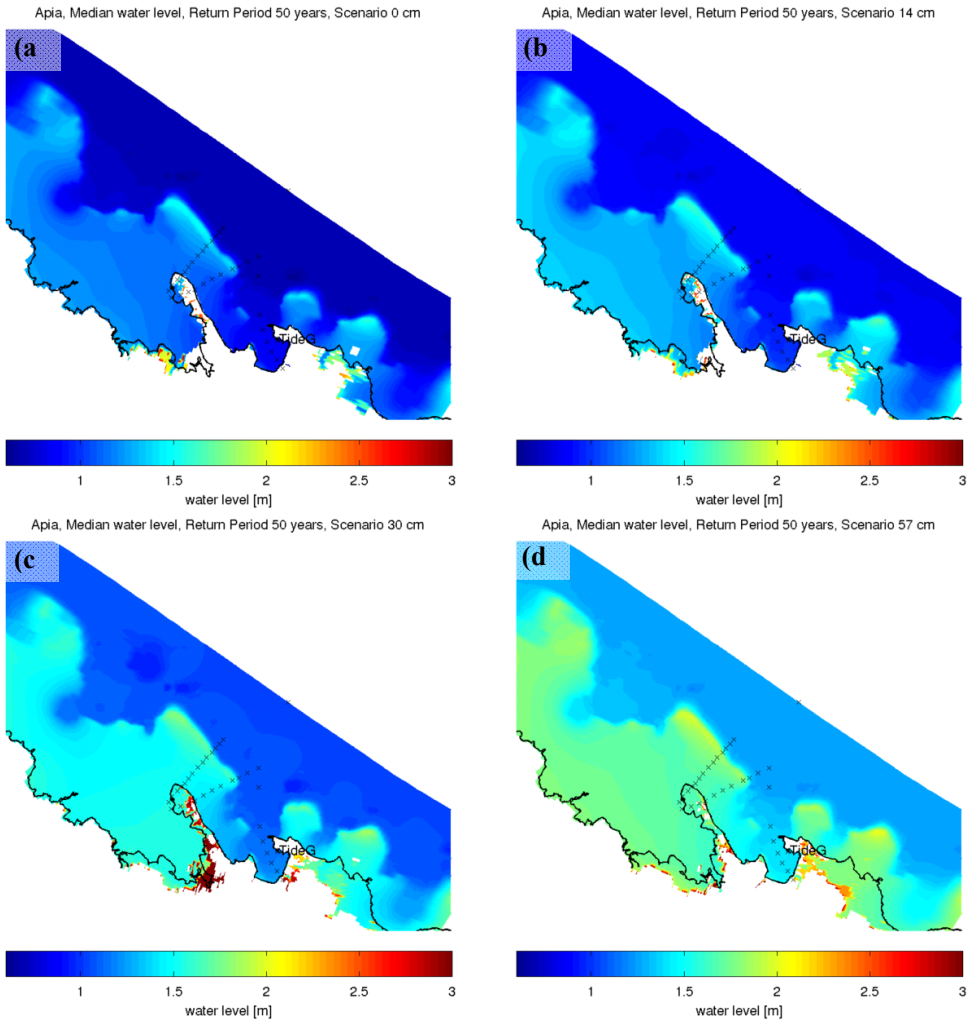

Fig. 18 Median value of the maximum modelled storm tide height (including wave setup) for the 1-in-50 year events under (a) baseline (1990), (b) 2030, (c) 2055 and (d) 2090 sea levels.

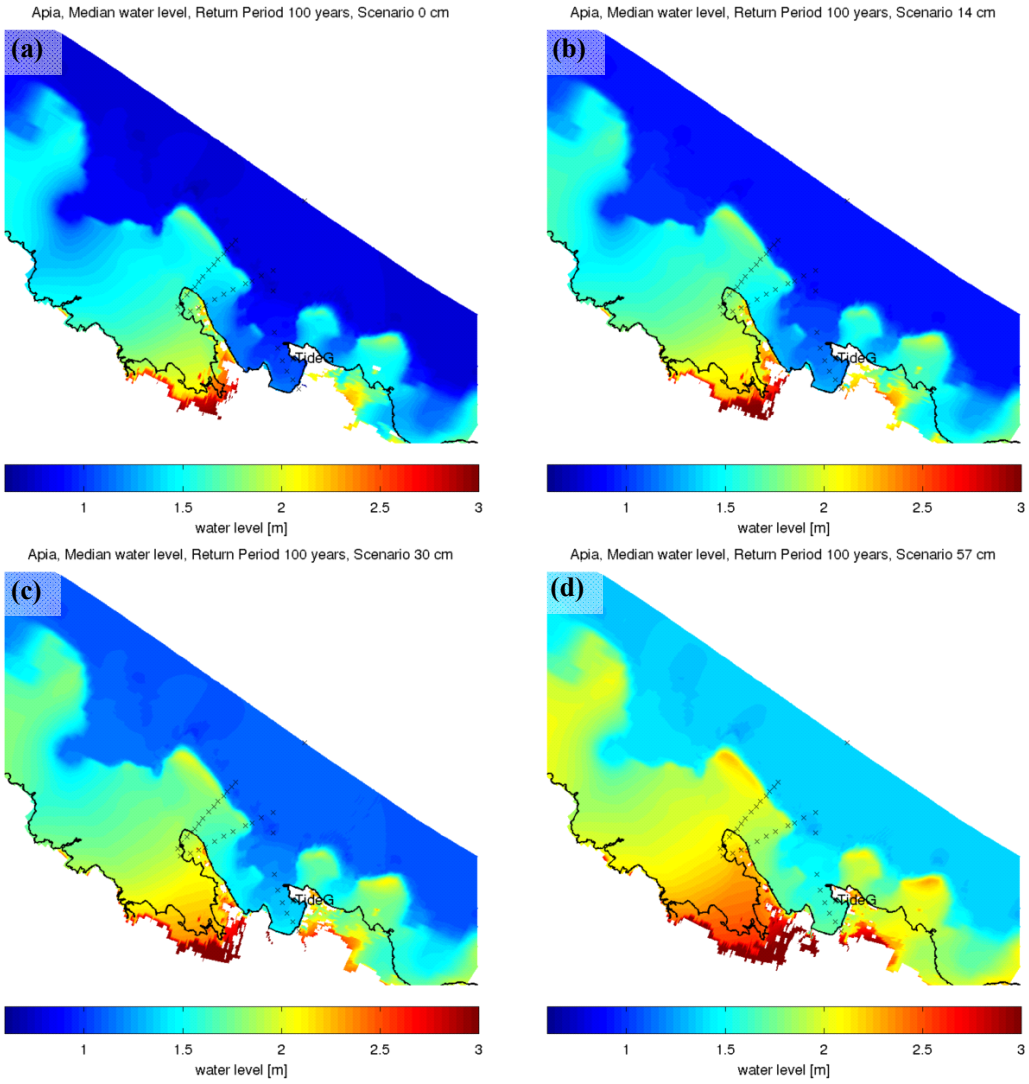

Fig. 19 Median value of the maximum modelled storm tide height (including wave setup) for the 1-in-100 year events under (a) baseline (1990), (b) 2030, (c) 2055 and (d) 2090 sea levels.

Figure 20 shows the median and maximum modelled depth averaged velocity for the 1-in-100 year storm tide under 1990 sea-level conditions and those projected for 2090. The strongest currents are evident in deeper waters immediately adjacent to the reef edges, as well is in the deeper harbour. Current speeds over the inundated parts of the Peninsula are small (less than 0.2 ms^{-1}) under median storm tide conditions, except at the narrowest part of the Peninsula where they reach 0.3 ms^{-1}. These values are similar in magnitude to those modelled for Tropical Cyclone Ofa (see previous section). In the modelled maximum situation, values of up to 1.0 ms^{-1} are evident, particularly across the narrowest section of the Peninsula. Under 2090 sea level conditions, a larger area of the Peninsula experiences depth-averaged velocities of around 1.0 ms^{-1}.

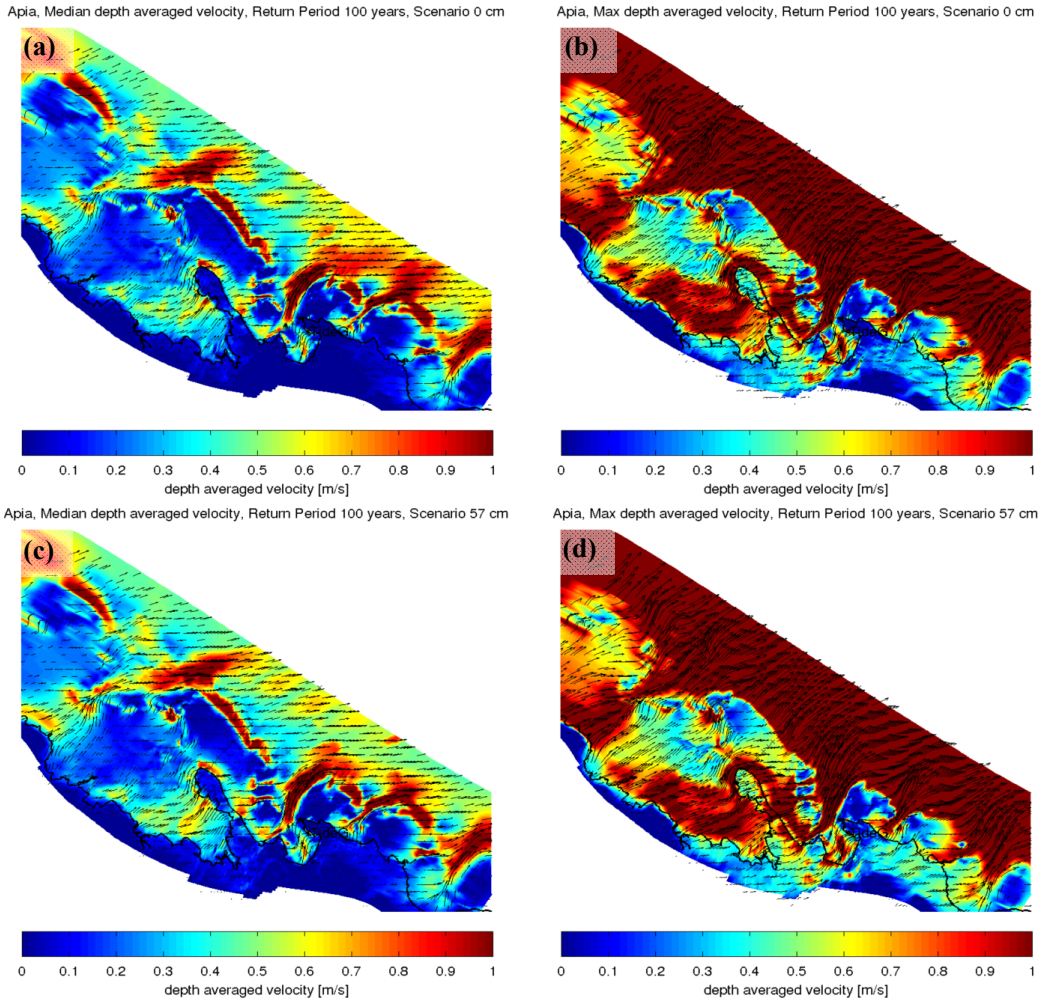

Fig. 20 (a) median and (b) maximum depth-averaged velocity from the 10-member ensemble of 100-year synthetic cyclone events under 1990 sea-level conditions and (c) median and (d) maximum depth-averaged currents under 2090 projected sea-level rise conditions.

A summary of median, minimum and maximum values of each simulation's maximum modelled wave height, significant wave height, and indicative current speed, averaged across two model points located immediately seaward of the eastern side of the Peninsula (see Fig. 9 for locations) is provided in Table 5.

5.3 Peninsula Model Results

To investigate the uncertainty in the results arising from the absence of observational data with which to calibrate the model, results are presented for three sets of plausible parameter settings, as discussed in Section 3. The range of incident wave heights and periods considered are 5.5 to 12 m and 8 to 12 s. It should be noted that the Peninsula Model was unable to simulate conditions at the longer wave periods (>12 s) indicated by the Apia Model (see Fig. 14). This is likely a failing in the underlying physics of the SWASH model: the very steep bathymetry, combined with longer wave lengths (periods), increases the importance of non-linear terms to the point of numerical instability. It is thus possible that the wave run-up,

overtopping and associated inundation is under-estimated by the Peninsula Model. This is despite the fact that, for reasons discussed in the wave setup section below, the Peninsula Model estimates higher wave setup than the Apia Model. To help address this shortcoming, results from a version of the Peninsula Model in which parameter settings have been combined to produce larger wave inundation were also produced. However, the upper bound of wave run-up and associated inundation remains poorly known. Hence estimates for such extreme conditions should be considered with this in mind.

Table 5 Summary of parameters from the Apia scale hydrodynamic and SWAN model simulations averaged across points located at the front of the seawall (points T1.10 and T2.7 in Fig. 9).

	Water level (m)	Significant wave height (m)	Depth-averaged currents (m/s)
Baseline			
20-yr	1.15 (0.69-1.43)	0.30 (0.15-0.42)	0.76 (0.40-1.02)
50-yr	1.39 (0.67-2.44)	0.41 (0.11-0.91)	0.81 (0.50-1.19)
100-yr	1.47 (0.90-1.99)	0.40 (0.13-0.85)	1.08 (0.54-1.69)
2030			
20-yr	1.32 (0.83-1.56)	0.38 (0.19-0.51)	0.79 (0.40-1.04)
50-yr	1.52 (0.81-2.56)	0.46 (0.14-0.98)	0.81 (0.50-1.19)
100-yr	1.60 (1.04-2.11)	0.46 (0.17-0.92)	1.08 (0.55-1.69)
2055			
20-yr	1.48 (0.99-1.71)	0.45 (0.25-0.59)	0.80 (0.41-1.05)
50-yr	1.68 (0.97-2.69)	0.53 (0.18-1.07)	0.82 (0.49-1.17)
100-yr	1.75 (1.20-2.25)	0.53 (0.21-1.01)	1.09 (0.56-1.68)
2090			
20-yr	1.74 (1.26-1.96)	0.58 (0.37-0.73)	0.82 (0.50-1.07)
50-yr	1.93 (1.23-2.94)	0.66 (0.26-1.22)	0.82 (0.47-1.13)
100-yr	2.00 (1.47-2.48)	0.66 (0.31-1.16)	1.09 (0.59-1.67)

Figure 21 shows the water levels from simulations that incorporate 1-in-100 year storm tide levels for 1990 and 2055, and under a range of possible wave conditions. The range of values for incident wave height and period considered for each scenario is given in columns 3 and 4 of Table 6, results from the Apia Model are given in column 5, and results from the Peninsula Model are presented in columns 6 to 8. An additional two sets of simulations were also undertaken with parameter settings combined to produce conditions conducive to a smaller amount of overtopping and inundation (Table 7) and a greater amount of overtopping and inundation (Table 8). These additional tables of results provide an indication of the sensitivity of the results to different, but plausible, parameter settings.

5.3.1 Wave Setup

Wave setup was modelled using both the 2D Apia Model and the Peninsula Model. Comparable values are provided in columns 5 and 6 of Tables 6 to 8. The values of the Apia scale model are typically lower by 0.3-0.5 m. This is likely to be partly due to the fact that the

model is of lower horizontal resolution and so does not resolve the sea wall and also that the model does not account for the generation of infragravity waves across the reef and wave run-up. However, it is important to also note that the Peninsula Model, being only 1D does not capture the complex two-dimensional flows that can lead to release of wave setup in the longshore direction across the reef flat and towards gaps in the reef (*ava* in Samoan) where seaward flowing strong rips out to deep water occur, reducing the overall wave setup at the coast. Therefore, both sets of results contain limitations that should be considered when interpreting the results.

Wave setup, or the increase in mean water levels due to wave dissipation (breaking), is primarily generated at two locations, at the reef edge and on the seawall. The contribution to total setup from the reef edge is captured in the 50th percentile water level at the 'toe' of the seawall and the contribution of wave setup from the face of the seawall. The total wave setup is within the rule of thumb 10-30% of the incident deepwater wave height (e.g. WMO, 1988; Tait, 1972; Vetter et al., 2010). For the minimum wave conditions considered (the low end of the range of wave conditions for the baseline 1-in-20 yr case of 5.5m H_s and 8 s T_p) breaking on the outer reef contributes 44% to the total wave setup at the coast, the other 56% from waves breaking on the seawall, but for larger waves and larger sea levels the seawall is more frequently overtopped and the contribution to wave setup from the sea wall is limited to 10% for the midrange wave conditions (i.e. 8.5-10.5m and 11s) and 1% for high range conditions (10-12m and 12s). At the lower end of the estimates, the 50th percentile water levels resulting from tropical cyclone conditions is on the order of 0.5 m below the seawall (~1.9m), and at the upper end the still water level including wave setup (but not run-up) is at the level of the height of the seawall (~2.4m).

The sensitivity in water level (including wave setup) due to the ensemble range of wave conditions (Table 6) can lead to variations of 30% between the low wave height case (5.5m 8s) to the midrange wave height case (8.5m 11s). Wave conditions for the upper end of the range (12m 12s) does not further increase the setup as the seawall is already inundated and the extra wave energy is converted into run-up and over-wash velocities.

Variations in model parameters lead to differences in the modelled water levels (Tables 7 and 8). Wave setup typically varies ±5% of the optimal tuning setting. With the 'low inundation' parameterization (Table 7) the 50 percentile water levels at the face tend to be lower by up to 7% from the 'optimal parameter' settings and could increase by up to 11% with the 'high inundation' parameters (Table 8).

5.3.2 Wave Run-up

Wave run-up height exceeded the seawall height (2.4m) for almost all modelled tropical cyclone scenarios as indicated by the black line on the seaward side of the seawall in Fig. 21. The height of the seawall limits the dynamical vertical run-up height to about 1m above the seawall (3.4 m), where for larger storms the wave momentum is transferred horizontally inland as over-wash cascading over the seawall. Higher water levels over the reef flat generate larger run-up on the seawall for a given incident wave height. The model sensitivity

to run-up is generally in the range of ±5% the optimal parameter settings value but can be as high as 10% due to the randomness of wave breaking of the highest top 2% of waves.

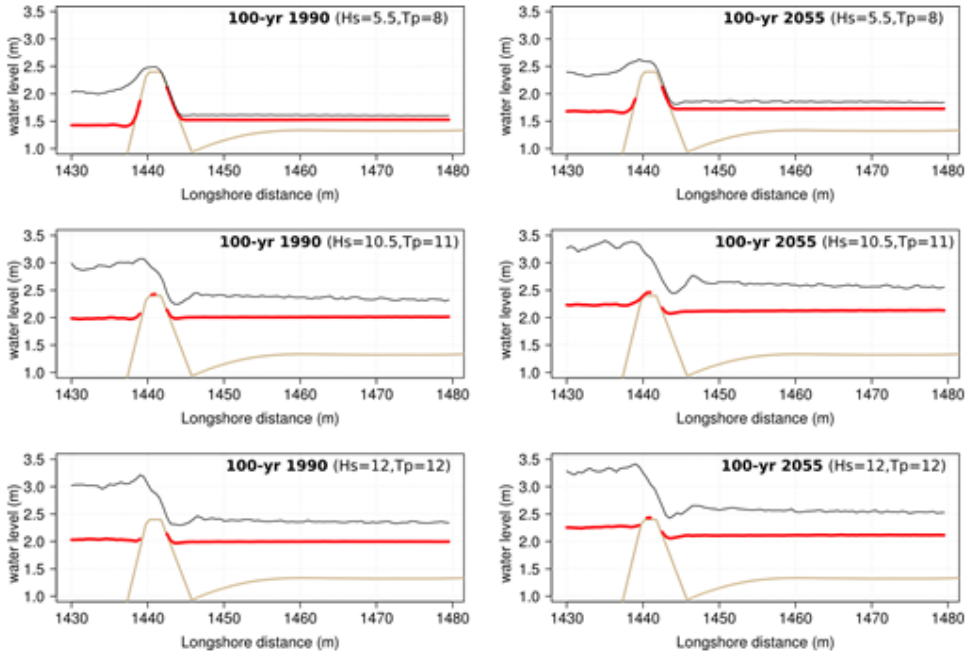

Fig. 21 Water levels simulated by the Peninsula Model for incident significant wave height (H_s) and peak period (T_p) indicated in parenthesis on each subplot. Red is 50th percentile sea level height and black is the 98th percentile height (i.e. water levels occurring 50% and 2% of the time during model runs). The seaward side of the Mulinu'u Peninsula is on the left side of the diagram with the seawall and the land level is indicated by the brown line. Water levels are relative to the 1973 MSL datum.

5.3.3 Maximum Velocity

When the overtopping from a tropical cyclone storm is excessive, the over-wash can generate large velocities at the seawall (as indicated in Fig. 22). These decline as the water moves inland. Typically velocities 30m inland are around 0.1 ms^{-1}, but the top 2% of velocities (possibly associated with infragravity waves generated by the over-wash) can be greater than 2 ms^{-1}. Comparing the values in Table 6 it can be seen that typically the 98th percentile velocities modelled for the low waves case (5.5 m and 8 s) were about 70% lower than the mid-range wave values (8.5 m and 11 s). The high waves case (12 m and 12 s) produced waves that were about 70% higher than the mid-range values. Comparing the results from Tables 6 to 8, the sensitivity in the 98th percentile value 30m inland is on the order of ±50% of the optimal parameters. The velocities can be 158% faster for the 'high inundation' compared to the optimal tuned settings, and 100% slower (near zero) for the 'low inundation' settings.

5.4 Representing Uncertainties

The model results shown in Tables 6 to 8 indicate a large spread in possible sea levels and velocities, depending on the incident wave conditions. The uncertainty in the Peninsula Model arising from the lack of observational data to calibrate the model increases this uncertainty still further, as indicated by the range of results between Tables 7 and 8. To provide a range of plausible values of water level and current speeds that encompass the key results across these dimensions of uncertainty, the results have been combined into a '*mid-range estimate*', with a range of values around this central estimate representing the uncertainty.

The basis of the '*mid-range estimate*' is the 98th percentile heights from the Peninsula Model since these encompass the contribution to water levels from storm tide, wave setup and wave run-up. The 50th percentile water levels from the Peninsula Model, were found to be of similar height (though slightly higher) to those simulated in the Apia Model and are taken to be at the '*low estimate'* of the range of estimated values since they do not account for the contribution to sea-level heights due to wave run-up. Similarly, 50th percentile velocities from the Peninsula Model were taken as the '*low estimate'*. Due to uncertainties around the lack of observations together with the limited range of wave periods investigated, the '*upper estimate'* of the range is taken from the Peninsula Model that combines plausible parameter settings so as to maximize the amount of inundation that could reasonably occur. The relevant values from Tables 6-8 are combined in this way in Table 9. For a 1-in-100 year storm tide the *mid-range estimate* (*lower estimate* - *upper estimate*) of sea level is around 2.4 (2.0 - 3.0) m in 1990, increasing to around 2.6 (2.1 - 3.1) m in 2090 and currents are around 1.2 (0.1 - 1.5) ms^{-1} in 1990 and increase to 1.5 (0.1 - 2.1) ms^{-1} in 2090 conditions.

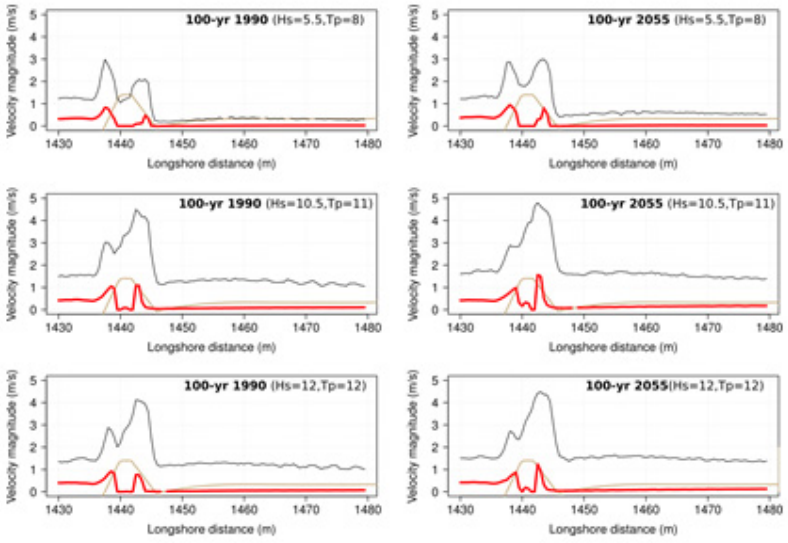

Fig. 22 Current velocities simulated by the Peninsula Model for the incident significant wave height (H_s) and peak period (T_p) indicated in parenthesis on each subplot. Red is 50th percentile velocity and black is the 98th percentile velocity (i.e. current magnitudes occurring 50% and 2% of the time during model runs). The seaward side of the Mulinu'u Peninsula is on the left side of the diagrams with the seawall and the land level indicated by the brown line.

Table 6 Summary of results modelled under optimum parameter settings of the Peninsula Model. All heights are relative to 1973 MSL. Column 1 is the return period and time horizon; column 2 is the incident water level (storm surge + tide + sea level); column 3 is the incident wave height and range; column 4 is the incident period; column 5 is the total water level in front of the sea wall modelled by the Apia Model for comparison with column 6, which is the median value of all points averaged over the region in front of the sea wall from the Peninsula Model (see Fig. 9); columns 7 and 8 are the median value and 98th percentile values (i.e. run-up) of heights over the face of the seawall

	WL	Hs	Tp	Apia Model	50p Toe	50p Face	98p Face
1990	**(m)**	**(m)**	**(s)**	**(m)**	**(m)**	**(m)**	**(m)**
20-yr	0.70	8.5 (5.5-10.0)	11.0 (8.0-12.0)	1.15 (0.69-1.43)	1.64 (1.22-1.73)	1.90 (1.87-1.89)	2.68 (2.25-2.72)
50-yr	0.84	9.5 (5.5-11.0)	11.0 (8.0-12.0)	1.39 (0.67-2.44)	1.83 (1.33-1.89)	1.97 (1.87-1.96)	2.92 (2.42-2.93)
100-yr	0.97	10.5 (5.5-12.0)	11.0 (8.0-12.0)	1.47 (0.90-1.99)	2.00 (1.43-2.05)	2.07 (1.87-2.04)	3.07 (2.48-3.21)
2030							
20-yr	0.84	8.5 (5.5-10.0)	11.0 (8.0-12.0)	1.32 (0.83-1.56)	1.77 (1.33-1.83)	1.93 (1.87-1.92)	2.79 (2.42-2.79)
50-yr	0.98	9.5 (5.5-11.0)	11.0 (8.0-12.0)	1.52 (0.81-2.56)	1.93 (1.44-2.00)	2.03 (1.87-2.01)	2.99 (2.48-3.07)
100-yr	1.11	10.5 (5.5-12.0)	11.0 (8.0-12.0)	1.60 (1.04-2.11)	2.10 (1.55-2.15)	2.13 (1.88-2.15)	3.25 (2.57-3.27)
2055							
20-yr	1.00	8.5 (5.5-10.0)	11.0 (8.0-12.0)	1.48 (0.99-1.71)	1.88 (1.46-1.93)	1.97 (1.87-1.97)	2.91 (2.50-2.93)
50-yr	1.14	9.5 (5.5-11.0)	11.0 (8.0-12.0)	1.68 (0.97-2.69)	2.06 (1.57-2.11)	2.13 (1.88-2.11)	3.19 (2.55-3.24)
100-yr	1.27	10.5 (5.5-12.0)	11.0 (8.0-12.0)	1.75 (1.20-2.25)	2.24 (1.69-2.27)	2.40 (1.91-2.29)	3.39 (2.63-3.41)
2090							
20-yr	1.27	8.5 (5.5-10.0)	11.0 (8.0-12.0)	1.74 (1.26-1.96)	2.08 (1.69-2.13)	2.14 (1.91-2.12)	3.12 (2.63-3.20)
50-yr	1.41	9.5 (5.5-11.0)	11.0 (8.0-12.0)	1.93 (1.23-2.94)	2.25 (1.79-2.30)	2.41 (1.95-2.36)	3.38 (2.72-3.44)
100-yr	1.54	10.5 (5.5-12.0)	11.0 (8.0-12.0)	2.00 (1.47-2.48)	2.32 (1.89-2.45)	2.36 (1.99-2.46)	3.35 (2.87-3.65)

Table 7 Summary of results modelled under 'low inundation' parameter settings of the Peninsula Model. All heights are relative to 1973 MSL. Column 1 is the return period and time horizon; column 2 is the incident water level (storm surge + tide + sea level); column 3 is the incident wave height and range; column 4 is the incident period; column 5 is the total water level in front of the sea wall modelled by the Apia Model for comparison with column 6, which is the median value of all points averaged over the region in front of the sea wall from the Peninsula Model (see Fig. 9); columns 7 and 8 are the median value and 98th percentile values (i.e. run-up) of heights over the face of the seawall.

	WL	Hs	Tp	Apia Model	50p Toe	50p Face	98p Face
1990	**(m)**	**(m)**	**(s)**	**(m)**	**(m)**	**(m)**	**(m)**
20-yr	0.70	8.5 (5.5-10.0)	11.0 (8.0-12.0)	1.15 (0.69-1.43)	1.62 (1.25-1.69)	2.10 (1.45-2.10)	2.68 (2.14-2.69)
50-yr	0.84	9.5 (5.5-11.0)	11.0 (8.0-12.0)	1.39 (0.67-2.44)	1.83 (1.36-1.90)	2.12 (1.77-2.13)	2.87 (2.29-3.01)
100-yr	0.97	10.5 (5.5-12.0)	11.0 (8.0-12.0)	1.47 (0.90-1.99)	2.02 (1.46-2.09)	2.19 (2.10-2.19)	3.09 (2.38-3.26)
2030							
20-yr	0.84	8.5 (5.5-10.0)	11.0 (8.0-12.0)	1.32 (0.83-1.56)	1.73 (1.36-1.79)	2.11 (1.77-2.10)	2.79 (2.29-2.79)
50-yr	0.98	9.5 (5.5-11.0)	11.0 (8.0-12.0)	1.52 (0.81-2.56)	1.93 (1.47-1.99)	2.15 (2.10-2.15)	2.99 (2.39-3.16)
100-yr	1.11	10.5 (5.5-12.0)	11.0 (8.0-12.0)	1.60 (1.04-2.11)	2.13 (1.58-2.18)	2.23 (2.10-2.23)	3.20 (2.63-3.40)
2055							
20-yr	1.00	8.5 (5.5-10.0)	11.0 (8.0-12.0)	1.48 (0.99-1.71)	1.85 (1.48-1.90)	2.12 (2.10-2.12)	2.84 (2.43-2.93)
50-yr	1.14	9.5 (5.5-11.0)	11.0 (8.0-12.0)	1.68 (0.97-2.69)	2.05 (1.60-2.12)	2.19 (2.10-2.20)	3.13 (2.64-3.21)
100-yr	1.27	10.5 (5.5-12.0)	11.0 (8.0-12.0)	1.75 (1.20-2.25)	2.24 (1.72-2.30)	2.31 (2.10-2.30)	3.36 (2.70-3.45)
2090							
20-yr	1.27	8.5 (5.5-10.0)	11.0 (8.0-12.0)	1.74 (1.26-1.96)	2.06 (1.72-2.12)	2.20 (2.10-2.20)	3.13 (2.70-3.13)
50-yr	1.41	9.5 (5.5-11.0)	11.0 (8.0-12.0)	1.93 (1.23-2.94)	2.28 (1.82-2.32)	2.33 (2.12-2.32)	3.29 (2.78-3.46)
100-yr	1.54	10.5 (5.5-12.0)	11.0 (8.0-12.0)	2.00 (1.47-2.48)	2.32 (1.94-2.51)	2.32 (2.15-2.71)	3.36 (2.87-3.67)

Table 8 Summary of results modelled under 'high inundation' parameter settings of the SWASH model. All heights are relative to 1973 MSL. Column 1 is the return period and time horizon; column 2 is the incident water level (storm surge + tide + sea level); column 3 is the incident wave height and range; column 4 is the incident period; column 5 is the total water level in front of the sea wall modelled by the Apia Model for comparison with column 6, which is the median value of all points averaged over the region in front of the sea wall from the Peninsula Model (see Fig. 9); columns 7 and 8 are the median value and 98th percentile values (i.e. run-up) of heights over the face of the seawall

	WL	Hs	Tp	Apia Model	50p Toe	50p Face	98p Face
1990	**(m)**	**(m)**	**(s)**	**(m)**	**(m)**	**(m)**	**(m)**
20-yr	0.70	8.5 (5.5-10.0)	11.0 (8.0-12.0)	1.15 (0.69-1.43)	1.63 (1.21-1.77)	1.88 (1.87-1.90)	2.73 (2.08-3.01)
50-yr	0.84	9.5 (5.5-11.0)	11.0 (8.0-12.0)	1.39 (0.67-2.44)	1.81 (1.32-1.97)	1.91 (1.87-2.00)	2.89 (2.28-3.22)
100-yr	0.97	10.5 (5.5-12.0)	11.0 (8.0-12.0)	1.47 (0.90-1.99)	1.96 (1.42-2.12)	1.99 (1.87-2.12)	3.16 (2.41-3.46)
2030							
20-yr	0.84	8.5 (5.5-10.0)	11.0 (8.0-12.0)	1.32 (0.83-1.56)	1.69 (1.32-1.89)	1.88 (1.87-1.95)	2.78 (2.28-3.12)
50-yr	0.98	9.5 (5.5-11.0)	11.0 (8.0-12.0)	1.52 (0.81-2.56)	1.91 (1.43-2.06)	1.97 (1.87-2.06)	3.10 (2.36-3.32)
100-yr	1.11	10.5 (5.5-12.0)	11.0 (8.0-12.0)	1.60 (1.04-2.11)	2.08 (1.53-2.21)	2.08 (1.87-2.20)	3.29 (2.51-3.61)
2055							
20-yr	1.00	8.5 (5.5-10.0)	11.0 (8.0-12.0)	1.48 (0.99-1.71)	1.84 (1.44-1.98)	1.93 (1.87-2.01)	3.03 (2.40-3.21)
50-yr	1.14	9.5 (5.5-11.0)	11.0 (8.0-12.0)	1.68 (0.97-2.69)	2.04 (1.39-2.15)	2.05 (1.87-2.16)	3.17 (2.52-3.54)
100-yr	1.27	10.5 (5.5-12.0)	11.0 (8.0-12.0)	1.75 (1.20-2.25)	2.20 (1.66-2.32)	2.21 (1.88-2.37)	3.44 (2.64-3.83)
2090							
20-yr	1.27	8.5 (5.5-10.0)	11.0 (8.0-12.0)	1.74 (1.26-1.96)	2.04 (1.66-2.18)	2.05 (1.88-2.19)	3.18 (2.64-3.45)
50-yr	1.41	9.5 (5.5-11.0)	11.0 (8.0-12.0)	1.93 (1.23-2.94)	2.20 (1.76-2.34)	2.20 (1.90-2.39)	3.40 (2.76-3.67)
100-yr	1.54	10.5 (5.5-12.0)	11.0 (8.0-12.0)	2.00 (1.47-2.48)	2.40 (1.87-2.50)	2.42 (1.95-2.51)	3.62 (2.87-3.90)

Table 9 Average and maximum sea levels and speeds attained on the landward side of the sea wall. The 50th percentile values (which are similar in value to the Apia Model values) are considered to be a 'low estimate' since transient wave action is not fully accounted for. The 'mid-range estimate' is taken to be the 98th percentile heights estimated from the Peninsula Model which includes the effects of transient wave activity. A plausible "upper estimate" is taken from the version of the Peninsula Model where the model parameter settings were combined to favour more extreme inundation. Water levels are relative to the 1973 MSL datum. Column 1 is the return period and time horizon; column 2 is the incident water level (WL: storm surge + tide + sea level); column 3 is the incident significant wave height and range (H_s); column 4 is the incident peak wave period (T_p).

				Water Levels			Current Speeds		
	WL	Hs	Tp	Low Estimate (50%)	Best Estimate (98%)	Upper Estimate (98% high)	Low Estimate (50%)	Best Estimate (98%)	Upper Estimate (98% high)
1990	**(m)**	**(m)**	**(s)**	**(m)**	**(m)**	**(m)**	**(m/s)**	**(m/s)**	**(m/s)**
20-yr	0.70	8.5 (5.5-10.0)	11.0 (8.0-12.0)	1.85 (NA-1.85)	1.99 (NA-2.04)	2.04 (NA-2.19)	0.04 (0.00-0.02)	0.80 (0.00-0.46)	0.58 (0.00-1.19)
50-yr	0.84	9.5 (5.5-11.0)	11.0 (8.0-12.0)	1.91 (1.40-1.94)	2.19 (1.45-2.22)	2.55 (1.40-2.88)	0.05 (0.02-0.07)	0.93 (0.27-1.08)	1.01 (0.15-1.63)
100-yr	0.97	10.5 (5.5-12.0)	11.0 (8.0-12.0)	2.00 (1.53-2.01)	2.37 (1.61-2.38)	3.01 (1.68-3.06)	0.08 (0.03-0.11)	1.25 (0.35-1.37)	1.51 (0.21-1.95)
2030									
20-yr	0.84	8.5 (5.5-10.0)	11.0 (8.0-12.0)	1.88 (1.40-1.90)	2.07 (1.45-2.16)	2.23 (1.45-2.48)	0.04 (0.02-0.06)	0.66 (0.27-1.02)	0.75 (0.15-1.34)
50-yr	0.98	9.5 (5.5-11.0)	11.0 (8.0-12.0)	1.95 (1.55-1.98)	2.26 (1.62-2.33)	2.87 (1.70-2.96)	0.06 (0.02-0.09)	1.09 (0.29-1.24)	1.32 (0.18-1.83)
100-yr	1.11	10.5 (5.5-12.0)	11.0 (8.0-12.0)	2.06 (1.66-2.07)	2.46 (1.73-2.48)	3.09 (1.90-3.12)	0.10 (0.02-0.14)	1.38 (0.43-1.42)	1.73 (0.23-2.12)
2055									
20-yr	1.00	8.5 (5.5-10.0)	11.0 (8.0-12.0)	1.92 (1.58-1.94)	2.17 (1.65-2.25)	2.52 (1.73-2.79)	0.05 (0.03-0.07)	0.94 (0.36-1.15)	1.12 (0.24-1.57)
50-yr	1.14	9.5 (5.5-11.0)	11.0 (8.0-12.0)	2.02 (1.69-2.04)	2.40 (1.80-2.42)	2.99 (1.92-3.02)	0.09 (0.03-0.12)	1.24 (0.55-1.37)	1.52 (0.27-2.00)
100-yr	1.27	10.5 (5.5-12.0)	11.0 (8.0-12.0)	2.12 (1.73-2.14)	2.57 (1.86-2.60)	3.18 (2.01-3.20)	0.13 (0.03-0.18)	1.53 (0.62-1.61)	1.93 (0.48-2.25)
2090									
20-yr	1.27	8.5 (5.5-10.0)	11.0 (8.0-12.0)	2.02 (1.73-2.03)	2.37 (1.86-2.40)	2.97 (2.01-2.99)	0.09 (0.03-0.11)	1.27 (0.62-1.31)	1.53 (0.48-1.90)
50-yr	1.41	9.5 (5.5-11.0)	11.0 (8.0-12.0)	2.13 (1.86-2.14)	2.60 (2.06-2.61)	3.13 (2.06-3.16)	0.14 (0.05-0.19)	1.58 (0.80-1.62)	1.85 (0.63-2.26)
100-yr	1.54	10.5 (5.5-12.0)	11.0 (8.0-12.0)	2.12 (1.91-2.24)	2.58 (2.16-2.77)	3.13 (2.30-3.32)	0.14 (0.07-0.22)	1.53 (1.01-1.79)	2.14 (0.80-2.48)

5.5 Discussion and Summary

In the present study, Samoa archipelago, Apia and Mulinu'u Peninsula scale numerical models were used to determine extreme sea levels around Apia under tropical cyclone forcing, with particular focus on the Mulinu'u Peninsula. To capture the range of wave conditions that can accompany storm tides of a given magnitude, a synthetic cyclone approach was used in which a Holland vortex model represented the wind and pressure fields over the model domains.

Results using the archipelago scale wave model were comparable to a well-validated global wave hindcast optimized for the South Pacific basin (Durrant et al., 2013) for historical cyclone events. This indicates that the Archipelago Model is capable of representing the wave field over deep ocean parts of the Samoan Archipelago. Comparisons of wave characteristics simulated using CFSR wind forcing during cyclone events and winds generated by the Holland vortex model showed good agreement for Cyclone Heta and Val. For Cyclone Ofa, the waves from the Holland winds were lower than those simulated using reanalysis wind forcing. This is attributed to the fact that the Holland vortex, while providing a good representation of the wind field associated with the cyclone, does not represent the far field winds as well. Ofa tracked to the west of Samoa and had a relatively large radius of maximum winds, so the Holland vortex representation of the wind field close to Apia was under represented. For Cyclone Tui, which tracked between Savai'i and Upolu, the wave heights simulated under the Holland vortex winds were higher than those simulated using reanalysis winds. For this cyclone, whose complex track also crossed Upolu (Fig. 3), it is likely that the Holland vortex captures the stronger winds near to the eye of the cyclone more realistically than is represented in the lower resolution CFSR wind data. It is therefore argued that the Holland vortex is likely to better represent the extreme waves arising from tropical cyclones that have paths that track closer to the location of interest. The synthetic storm tide modelling study demonstrated that the majority of cyclones contributing to extreme storm tide conditions, excluding wave effects, were the closer tracking cyclones. For this reason the Holland vortex model is appropriate for representing the wind and pressure fields. No systematic difference was found between wave fields generated by historical re-analysis winds or Holland vortex winds.

The archipelago to Apia scale models also showed a high degree of skill in simulating water levels both at the location of the tide gauge and at the location of the SPC-SOPAC ADCP at the entrance to the harbour during non-tropical cyclone conditions. Simulations of historical tropical cyclones also compare favourably with storm surge measured at the tide gauge, as well as with historical accounts of inundation. For instance, maximum water levels simulated during Cyclone Ofa led to inundation of much of the Mulinu'u Peninsula and the adjacent coastal strip to the west from Vaiusu to Fugalei. Significant inundation was also shown for the coast at Vaipuna to the east of Apia Harbour. These areas of inundation are consistent with anecdotal accounts and published reports, e.g. Rearic (1990).

The Apia Model simulations revealed distinct spatial patterns of waves and local sea level that emerge in response to the variations in bathymetric depths offshore. Considerable wave dissipation occurs at the reef edge, leading to a dramatic reduction in wave height over the reef flats and to a large increase in water level due to wave setup at the adjacent coastlines. The absence of reefs across the mouth of the harbor allows for significant wave penetration into the

harbor. This also results in very little wave setup within the harbor where the tide gauge is located and time-averaged sea levels in both model simulations and in the actual tide gauge observations do not increase significantly beyond those imposed at the offshore boundary due to astronomical tides and storm surge (e.g. Figs 16 and 17). This is consistent with the findings of Hoeke et al., (2013a), who report on a significant wave-driven inundation event during which tide gauge measurements indicated little to no evidence of an increase in local water level above normal tide levels. Wave setup was not the only contributor to relatively large local variations: wind setup was found to significantly elevate sea level in Vaiusu Bay, to the west of Mulinu'u Peninsula, under tropical cyclone conditions, relative to Apia Harbour. However, wave heights were found to be at a minimum within Vaiusu Bay, so while locally elevated water levels may inundate the peninsula from this side, overtopping of the embankments along the western side by waves is not expected to be significant relative to the eastern (seaward) side's seawall.

The Peninsula Model illustrated the potential importance of individual waves to overtop the seawall, greatly increasing the degree of inundation over that of storm tide and wave setup alone. While time-averaged (i.e. ~half hourly) water levels simulated by both the Apia and Peninsula models were essentially similar, instantaneous water levels simulated by the Peninsula Model were considerably higher. These waves often overtopped the seawall, causing ponding behind the seawall and in more extreme cases created bore-like infragravity waves which surged across the peninsula. Such bores have the potential to be extremely damaging to buildings and other infrastructure (e.g. Blacka et al. 2013). While these are represented in the 98th percentile water level and current velocity results (e.g. Fig. 21, Fig. 22 and Table 9), the ability of the model to accurately represent the heights and speeds of such infragravity motions should be treated with caution, for the reasons outlined below.

It is important to note that numerical limitations in the Peninsula Model prevented the modelling of incident wave periods longer than 12 s, predicted to occur by the Apia Model. It is thus possible that the wave run-up, overtopping and associated inundation is under-estimated by the Peninsula Model. This can be partially ameliorated by selecting results from the version of the model with parameter settings combined to cause a greater amount of overtopping and inundation (e.g. Table 8). However, the upper bound of wave run-up and associated inundation remains poorly known and should be treated with caution. Furthermore, the potential for the rocks used in the Apia's seawall revetment to become projectiles under extreme cyclone wave conditions was not simulated and remains an unknown, potentially destructive hazard.

Modelled components of water levels from the Peninsula Model at the seawall under baseline (1990) conditions are summarized in Fig. 23. The median (50th percentile) water level from the model is taken to represent storm tide+wave setup. Values that are attained 2% of the time (98th percentile) during each storm event simulation are taken to represent the combined sea level due to storm tide, wave setup and instantaneous water level height, whether due to wave height, wave run-up or infragravity waves. The importance of wave processes is clearly demonstrated with wave setup adding on the order of an additional 1 m of sea level to the storm tide levels considered. Wave run-up increases the instantaneous sea levels by about another 1 m. The run-up contribution is slightly lower in the 1-in-100 year case, because the water levels have exceeded the height of the seawall and so less energy goes into run-up and more into overtopping the seawall.

The results of two earlier storm tide studies are also shown in Fig. 23. These compare well with the results of the current study. Carter (1987) estimated a 1-in-100 year storm tide level of 0.92 m, by combining an estimate of 0.72 for a 1-in-100 year storm surge with a tide height of 0.2m, yielding a value very close to that estimated for the present study based on statistical and numerical modelling. Assuming an incident (offshore) wave height of 11.3 m, a period of 13.6 s, Carter estimated wave setup based on two different empirical approaches. The first, based on the formulation of Seelig (1983), yielded a value of 1.11m. The second, based on US Corps. of Engineers (1977), yielded a value of 1.40 m. The optimal values determined in the present study coincide with the lower end of this range.

The storm tide estimates of Beca (2001) for 20 to 100-year levels are around 50% higher than those modelled in the present study, partly because a maximum spring tide value of 0.5 m was added to their estimated values of storm surge height. The results of the present study suggest that the levels adopted by Beca (2001) for 20, 50 and 100-year levels would more realistically occur with return periods of 300, 500 and 900 years respectively. Values of wave setup in the study of Beca (2001) are also considerably higher than both the values modelled in the present study and those of Carter (1987). The Beca values are more closely aligned with the maximum values estimated in the present study that are reached around 2% of the time due to the additional effect of wave run-up.

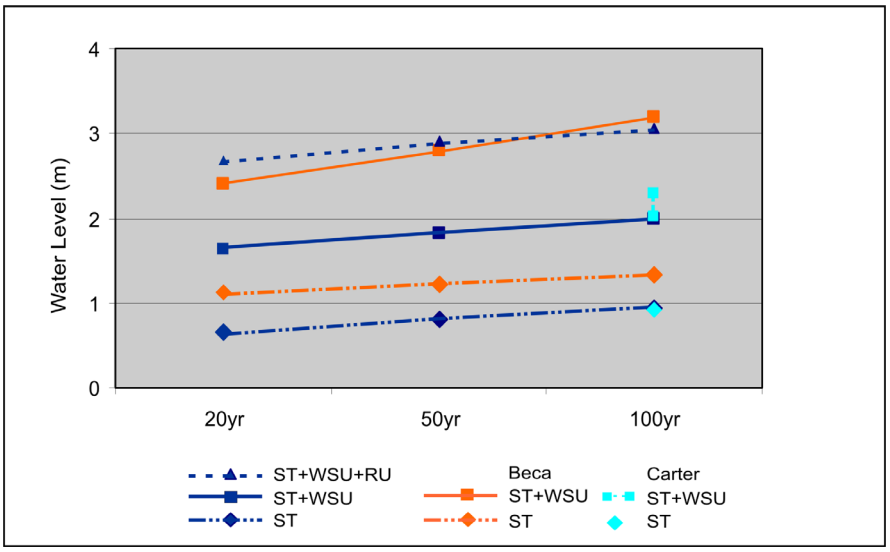

Fig. 23 Comparison of modelled water levels for 20, 50 and 100-year return period levels for baseline (current climate) sea level in the present study (dark blue symbols) with those estimated in two previous studies - Values estimated by Beca (2001) and Carter (1987) are shown in orange and light blue, respectively. ST refers to storm tide, WSU refers to wave setup and RU refers to run-up. Water levels are relative to the 1973 MSL datum. Note that the ST+WSU+RU water levels plotted correspond to the mid-range estimates of the Peninsula Model.

Indicative water levels and current speeds behind the seawall, determined for 50- and 100-year storm tides for both baseline and future sea level rise scenarios, are shown in Fig. 24. The median values (50th percentile) from the Peninsula Model were consistent with water levels

simulated by the Apia Model and were considered to be a *lower estimate* since they do not account for wave run-up and overtopping. To provide a *mid-range estimate* of water levels and current speed, the additional sea-level height due to run-up is estimated using the Peninsula Model and is added to the Apia Model results. Since the *mid-range estimates* incorporate ensemble averages from the Apia Model and run-up from the Peninsula Model, they are considered the best, or most likely estimates at the Mulinu'u Peninsula. However, the complexity of wave run-up and overtopping of the seawall, combined with a lack of observational data, results in significant uncertainty in these. To illustrate uncertainty in the model results due to the absence of observational data for calibrating the models as well as the contribution from longer period incident waves that were not accounted for in the Peninsula Model, an *upper estimate* of sea level is obtained using results from the Peninsula Model where model parameter settings were combined to favour more extreme inundation. For a 1-in-100 year storm tide the *mid-range estimate* (*lower estimate* - *upper estimate*) of sea level is around 2.4 (2.0 - 3.0) m in 1990, increasing to around 2.6 (2.1 - 3.1) m in 2090 and currents are around 1.2 (0.1 - 1.5) ms^{-1} in 1990 and increase to 1.5 (0.1 - 2.1) ms^{-1} in 2090 conditions.

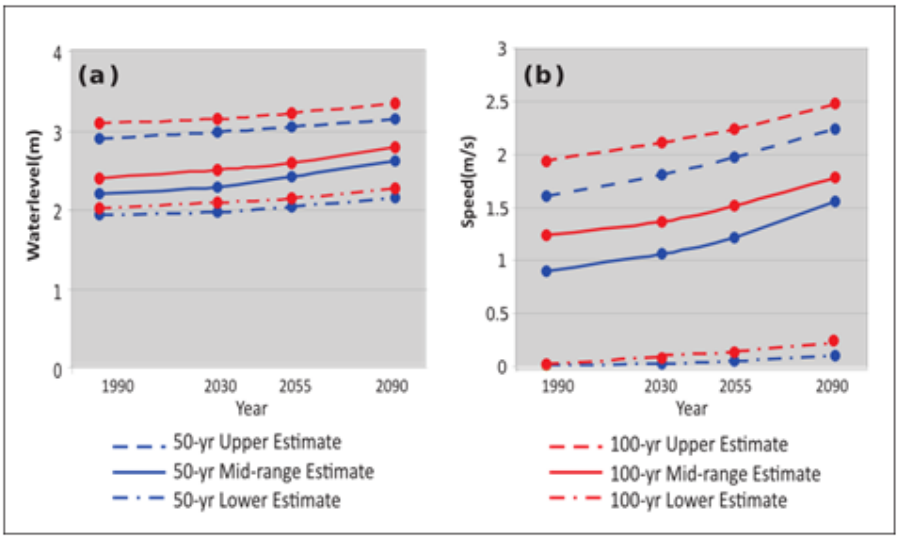

Fig. 24 Average and maximum (a) sea levels and (b) speeds attained on the landward side of the seawall under future scenarios of sea-level rise. The low estimate values are derived from the Apia Model since they do not include the effects of transient wave activity (i.e. wave run-up and overtopping). The mid-range estimate is derived by adding to the Apia Model results the difference in the 50th and 98th percentile heights estimated from the Peninsula Model, to account for the effects of transient wave activity. The upper estimate is derived in the same way as the mid-range estimate but using the Peninsula Model values where the parameter settings favoured more extreme inundation. Water levels are relative to the 1973 MSL datum.

Results of the Apia Model highlight the areas of Apia that are at risk of inundation. The inland extent of the modelled inundation is shown in Fig. 25 for the 50 and 100-year storm tides under the different scenarios of sea-level rise. Some degree of inundation of the Mulinu'u Peninsula is evident for all scenarios considered, with the greatest extent clearly occurring for the 100-year

storm tide. In the Apia Model, the inundation tended to occur from the western side of the Peninsula and increasingly covered the entire peninsula for the higher storm surge levels (i.e. the 1 in 100 year event) and future sea-level rise scenarios. This was due to high wind setup in Vaiusu Bay when the cyclone track brought strong westerly winds near the peak of the storm tide. However, the Apia Model's inability to account for individual waves overtopping the seawall likely greatly under represents inundation of the peninsula from the seaward (eastern) side. In the Peninsula Model, overtopping of the sea wall by individual waves was important, leading to significant inundation from the seaward side and high instantaneous water velocities on the peninsula itself. In reality, wind setup in Vaiusu Bay (captured by the Apia Model) and wave overtopping of the seawall (not captured by the Apia Model) are likely both significant contributors to inundation of the Mulinu'u Peninsula, with their relative importance dependent on the particular track, intensity and speed of the tropical cyclone. The Apia Model also predicted significant inundation at 50 and 100-year return periods along the adjacent coastal strip from Fugalei to Vaiusu, as well as increasingly significant inundation under increasing storm severity around Vaipuna on the eastern side of town under higher sea-level rise scenarios. Risks of overtopping of the Apia seawall away from the Mulinu'u Peninsula were not directly modelled and therefore remain unquantified. This risk may be especially significant in Apia Harbor. In the Apia Model results (e.g. Fig.ES3a and Fig.16) the Harbour experiences significant wave penetration closer to shore compared to surrounding areas.

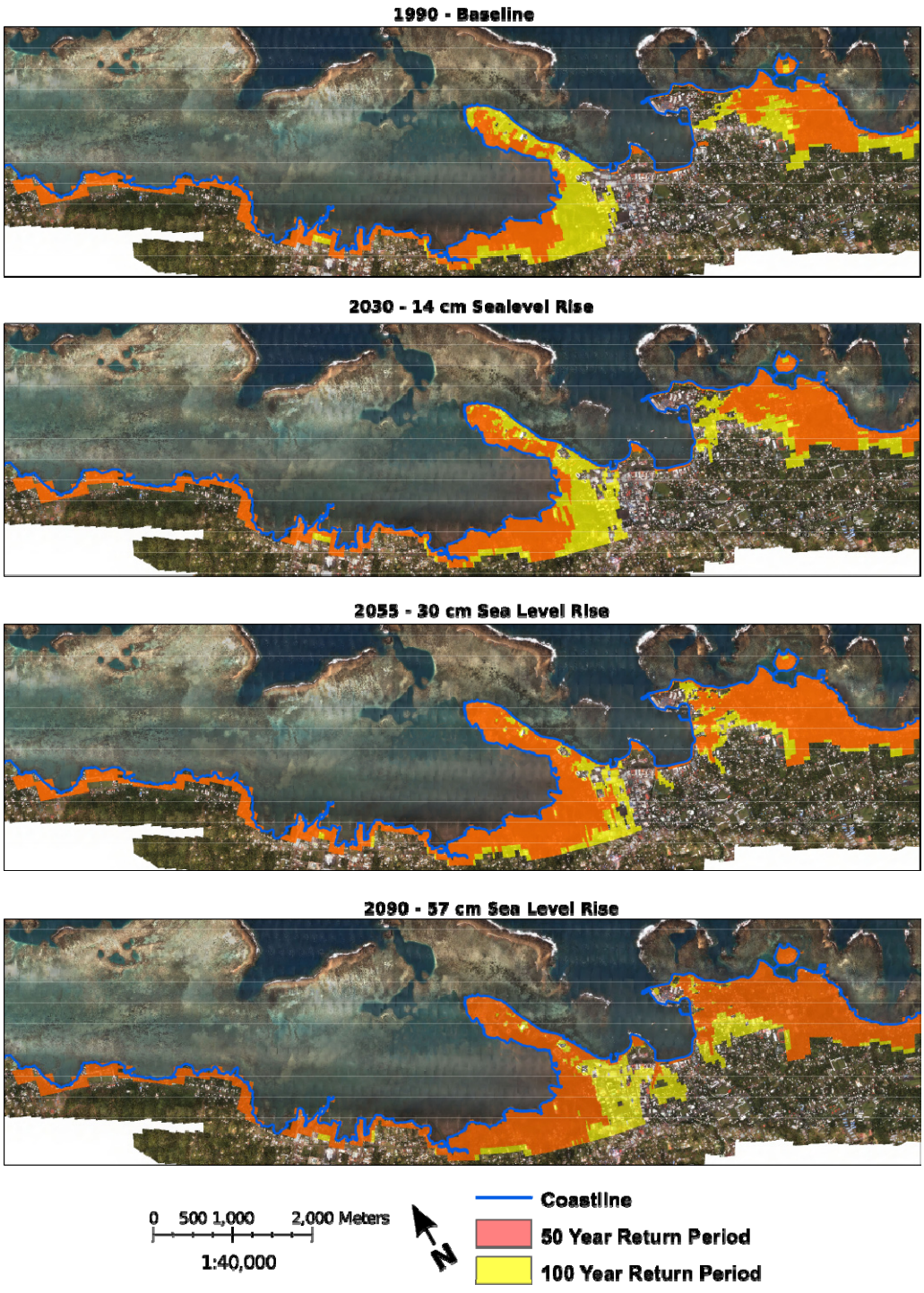

Fig. 25 The area inundated, as estimated by the Apia Model (storm tide and wave setup), for 50 year and 100 year return period storms under 1990 (baseline) and 2030, 2055 and 2090 future sea -level scenarios.

6. CONCLUSIONS AND RECOMMENDATIONS

This study has resulted in estimates of coastal inundation risk from tropical cyclones at a scale meaningful to infrastructure design and civil planning for the city of Apia and, in particular, the Mulinu'u Peninsula. They were derived by dynamically downscaling relevant atmospheric and marine information and simulating relevant processes. A hierarchy of hydrodynamic wind-wave and circulation models were implemented at the archipelago scale and the scales of Apia and of the Mulinu'u Peninsula. These models were used to investigate the contributions to coastal extreme sea levels from astronomical tides and storm surge (i.e. inverse barometer effect and wind setup), as well as wind-wave generation and nearshore wave breaking, leading to coastal wave setup and wave run-up.

The modelling work presented in this study represents a significant step forward in the quantification of storm tide risk modelling for the Apia coastline. Modelling at the scale of Apia and the Mulinu'u Peninsula relies on high quality geophysical data and as such would not be possible without the high resolution coastal bathymetry and topography (LiDAR) data recently acquired for the Apia area.

Results indicated that areas of Apia are highly vulnerable to inundation during tropical cyclones. Future increases in mean sea level will exacerbate that risk. The Mulinu'u Peninsula is particularly vulnerable. Under present climate conditions the findings indicate that significant inundation would result from a 1-in-50 year tropical cyclone event and complete inundation would occur for a 1-in-100 year event. With future increases in sea level, complete inundation of the peninsula will be achieved under less extreme conditions. Model results indicate that for a 1-in-100 year storm tide, including future projected sea-level rise, sea levels on Mulinu'u Peninsula may reach 2.4 m above current mean sea level by 2055. While specifically evaluating design considerations of coastal protection for the Mulinu'u Peninsula (such as those recommended in Hay and Hartley, 2013) is beyond the scope of this study, the results of this study can provide the basis for such an evaluation.

The wave heights and periods simulated from the synthetic cyclone winds produced a range of values that spanned those that have occurred during notable historical cyclone events since 1990 as well as larger but nevertheless plausible wave heights than have been observed during this period. It should be noted, however, that estimates of storm risk for Apia are still subject to large uncertainty. Although the large uncertainty range of modelled wave conditions for each return period could be narrowed further by increasing the ensemble size in the synthetic modelling of cases, a number of other important factors contributing to the uncertainty are highlighted. These are: (1) the paucity of observational data on deepwater waves (e.g. offshore wave buoys in the region), with which to calibrate and validate the modelling; (2) the short length (20 years) of tide gauge data from the point of view of sampling tropical cyclone-induced extreme water levels; and (3) the absence of nearshore observational data on water levels and wave transformation processes across the reefs surrounding Apia Harbour, and in front of Mulinu'u Peninsula, in particular. With regards to (3), investment in *in situ* observations of waves, water levels and currents, particularly over shallow reef flats where wave setup may elevate local water levels up to a metre or more, would provide data essential to the calibration

of high resolution models such as the Apia and Peninsula models used in the present study. This is important since these locations have been shown to experience local water levels that are considerably higher than those (both modelled and measured) at the tide gauge during storms.

In summary, the models and methods employed in this study have demonstrated a major advance in the ability to provide credible information for use in infrastructure design and adaptation planning for future sea-level rise conditions. However, future studies, both in Apia and elsewhere in the Pacific, would benefit from the following recommendations:

1. High-resolution coastal bathymetry and topography, particularly of shallow reef areas, needs to be identified as essential to informing coastal risks; such information is ideally provided by LiDAR surveys, but can also be supplied by ground-based surveys and satellite-derived bathymetry.
2. Appropriate consideration should be given to the complexity of coastal inundation risk analysis and the associated timelines and costs, particularly given accepted sea level rise/climate change scenarios;
3. Investment in *in situ* observations of waves, water levels and currents should be made, particularly over shallow reef flats where wave setup may considerably elevate local water levels up to a metre or more; such observations are essential for prediction of local vulnerabilities to wave- and wind- driven extreme sea levels and are typically not captured by tide gauges. They are necessary to reduce uncertainty of both simple empirical tools as well as complex numerical models.

REFERENCES

Arcement, G. and Schneider, V. 1989. Guide for selecting Manning's roughness coefficients for natural channels and flood plains. Retrieved from http://mosfet.isu.edu/classes/Sato/ENVE615/S13/Manning n.pdf

Australian Bureau of Meteorology and CSIRO. 2011. Climate Change in the Pacific: Scientific Assessment and New Research. Volume 1: Regional Overview. Volume 2: Country Reports, 530 pp.

Beca, 2001. Input Data for Economic Analysis. Prepared for Government of Samoa, Department of Lands, Surveys and Environment. Beca International Consultants Ltd, 37pp.

Blacka, M., Flocard, F., Rayner, D., Rahman, P. and Parakoti, B. 2012. 1, A Case Study of Vulnerability to Cyclones and Climate Change: Avarua, Rarotonga. UNSW Report.

Booij, N., Ris, R.C. and Holthuijsen, H.L. 1999. A third-generation wave model for coastal regions, Part I, Model description and validation, J. Geophys. Res., 104(C4), 7649-7666.

Buckley, M. and Lowe, R. 2013. Evaluation of nearshore wave models in steep reef environments. Coastal Dynamics 2013, 249-260. Retrieved from www.coastaldynamics2013.fr/pdf_files/023_Buckley_Mark.pdf

Carter, R. 1987. Design of the Seawall for Mulinu'u Point, Apia, Western Samoa. SOPAC Technical Report 78, SOPAC, Suva, Fiji, 30pp.

Church, J. and White, N. 2011. Sea-Level Rise from the Late 19th to the Early 21st Century. Surveys in Geophysics, 32(4-5), 585-602.

Church, J.A., White, N.J. and Hunter, J.R. 2006. Sea-level rise at tropical Pacific and Indian Ocean islands. Global and Planetary Change 53, 155-168.

Codiga, D.L. 2011. Unified Tidal Analysis and Prediction Using the UTideMatlab Functions. Graduate School of Oceanography, University of Rhode Island, Narragansett, RI.

Cogley, J.G. 2009. Geodetic and direct mass-balance measurements: comparison and joint analysis. Annals of Glaciology 50.50 (2009): 96-100.

Durrant T., Greenslade, D., Hemer, H. and Trenham, C. 2014. A Global Wave Hindcast focussed on the Central and South Pacific. CAWCR Report. Australian Bureau of Meteorology and CSIRO.

Filipot, J.F. and Cheung, K. F. 2012. Spectral wave modeling in fringing reef environments, Coastal Engineering 67: 67-79.

Hay, J.E. and Hartley, P. 2013. Climate Risk and Adaptation Assessments for the Samoa Parliament Complex Redevelopment Project. Final Report. 70 pp.

Hoeke, R.K., McInnes, K.L., Kruger, J., McNaught, R., Hunter, J. and Smithers, S. 2013a. Widespread inundation of Pacific islands by distant-source wind-waves. 108, 128–138.

Hoeke, R.K., Storlazzi, C.D. and Ridd, P.V. 2013b. Drivers of circulation in a fringing coral reef embayment: A wave-flow coupled numerical modeling study of Hanalei Bay, Hawaii." Continental Shelf Research. 58,79-95.

Hoeke, R. K., Storlazzi, C. D. and Ridd, P.V. 2011. Hydrodynamics of a bathymetrically complex fringing coral reef embayment: Wave climate, in situ observations, and wave prediction, J. Geophys. Res., 116(C4), 1978–2012.

Holland, G.2008. A revised hurricane pressure–wind model. Monthly Weather Review 136, 3432-3445.

Holland, G.J., Belanger, J.I. and Fritz, A. 2010. A revised model for radial profiles of hurricane winds. Monthly Weather Review 138, 4393–4401.

Holland, G.J.1980. An analytic model of the wind and pressure profiles in hurricanes. Monthly Weather Review 108, 1212-1218.

Hubert, G.D. and McInnes, K.L. 1999. A storm surge inundation model for coastal planning and impact studies. Journal of Coastal Research 15, 168-185.

Japan International Cooperation Agency (JICA). 1993. Basic design study report on the project for rehabilitation and improvement of cyclone-damaged ports and foreshore protection in Western Samoa. 248pp.

Jaramillo, S. and Geno, P. 2011. AUV-based bed roughness mapping over a tropical reef. Coral Reefs 30.1:11-23.

Kennedy, A.B. et al., 2012. Tropical cyclone inundation potential on the Hawaiian Islands of Oahu and Kaua. Ocean Modelling 52–53, 54-68.

Komen, G.J., Hasselmann, S. and Hasselmann, K. 1984. On the existence of a fully developed wind-sea spectrum, J. Phys. Oceanogr., 14, 1271-1285.

Kossin, J.P., Knapp, K.R., Vimont, D.J., Murnane, R.J. and Harper, B.A. 2007. A globally consistent reanalysis of hurricane variability and trends. Geophysical Research Letters 34(L04815).

Le Provost, C., Genco, M.L. and Lyard, F. 1995. Modeling and predicting tides over the World Ocean." Quantitative skill assessment for coastal ocean models (1995): 175-201.

Lesser, G.R., Roelvink, J.A., van Kester, J.A.T.M. and Stelling, G.S. 2004. Development and validation of a three-dimensional morphological model, Coastal Engineering, 51(8-9), 883-915.

Lowe, R J., Falter, J.L., Bandet, M.D., Pawlak, G., Atkinson, M.J., Monismith, S.G. and Koseff, J.R. 2005. Spectral wave dissipation over a barrier reef, J. Geophys. Res., 110, C04001.

McInnes, K.L., Walsh, J.E., Hoeke, R.K., O'Grady, J.G., Hubbery, G.D. and Colberg,F. (in review). Quantifying Storm Tide Risk in Fiji due to Climate Variability and Change. Global and Planetary Change.

Madsen, O.S., Poon, Y.-K. and Graber, H.C. 1988. Spectral wave attenuation by bottom friction: Theory, Proceedings of 21th International Conference on Coastal Engineering, Am. Soc. of Civ. Eng., New York.

Meehl, G.A. et al., 2007. The WCRP CMIP3 multimodel dataset: A new era in climate change research." Bulletin of the American Meteorological Society 88.9 (2007): 1383-1394.

Merrifield, M.A. and Genz, A.S. et al. 2013. Annual maximum water levels from tide gauges: Contributing factors and geographic patterns. Journal of Geophysical Research: Oceans 118(5): 2535-2546.

Mulligan, R.P., Bowen, A.J., Hay, A.E., Westhuysen, A.J. v. d. and Battjes, J.A. 2008a. Whitecapping and wave field evolution in a coastal bay, J. Geophys. Res., 113, C03008.

Mulligan, R.P., Hay, A.E. and Bowen, A.J. 2008b. Wave-driven circulation in a coastal bay during the landfall of a hurricane, J. Geophys. Res., 113, C05026.

Nakicenovic, N. et al. 2000. Special report on emissions scenarios: a special report of Working Group III of the Intergovernmental Panel on Climate Change. No. PNNL-SA-39650. Pacific Northwest National Laboratory, Richland, WA (US), Environmental Molecular Sciences Laboratory (US), 2000.

Pelydryn, A. 2012. Acquisition of LiDAR and Imagery Derived Products for Samoa, (Cmc).

Rahmstorf, S., Cazenave, A., Church, J.A., Hansen, J.E., Keeling, R.F., Parker, D.E. and Somerville**,** R.C.J. 2007. Recent climate observations compared to projections. Science, 316, 709.

Rearic, D.M. 1990. Survey of Cyclone Ofa damage to the northern coast of Upolu, Western Samoa. SOPAC Technical Report 104. 36pp.

Ris, R., Holthuijsen, L. and Booij, N. 1999. A third-generation wave model for coastal regions: 2. Verification, J. Geophys. Res., 104, 7667- 7681

Roelvink, J.A. and v. Banning, C.K.F.M., 1994. Design and development of DELFT3D and application to coastal morphodynamics, in Hydroinformatics '94, edited by A. Verwey, A.W. Minns, V. Babovic and C. Maksimovic, Balkema, Rotterdam, Balkema, Rotterdam.

Roelvink, J.A. and Wasltra, D.J. 2004. Keeping in simple by using complex models, in 6th International Conference on Hydroscience and Engineering, Advances in Hydro-Science and Engineering, edited, Brisbane, Australia., Brisbane, Australia.

Saha, S. et al. 2010. The NCEP Climate Forecast System Reanalysis. Bulletin of the American Meteorological Society, 91(8), pp.1015–1057.

Seelig, W.N. 1983. Laboratory study of reef-lagoon system hydraulics. Journal of Waterways, Port, Coastal and Ocean Engineering. Vol. 109, No. 4.

Solomon, S.M. 1994. A review of coastal processes and analysis of historical coastal change in the vinicity of Apia, Western Samoa. SOPAC Technical Report 208. 62pp.

Taebi, S., Lowe, R.J., Pattiaratchi, C.B., Ivey, G.N. and Symonds, G. 2012. A numerical study of the dynamics of the wave-driven circulation within a fringing reef system. Ocean Dynamics 62 (4), 585-602

Tait, R.J. 1972. Wave Set-Up on Coral Reefs. Journal of Geophysical Research, 77(12), 2207-2211.

US Corp of Engineers. 1977. Shore Protection Manual, Vols. I and II. U. S. Army Coastal Engineering Research Center, Kingman Building, Fort Belvoir, Virginia 22060, Third Edition.

Vetter, O. et al. 2010. Wave setup over a Pacific Island fringing reef. Journal of Geophysical Research, 115(C12), C12066.

Walsh, K.J.E., McInnes, K.L. and McBride, J.L. 2012. Climate change impacts on tropical cyclones and extreme sea levels in the South Pacific — A regional assessment. Global and Planetary Change 80–81, 149-164.

WMO, 1988. Guide to wave analysis and forecasting. World Meteorological Organization, Report No. 702.

Zijlema, M. 2012. Modelling wave transformation across a fringing reef using SWASH. Coastal Engineering Proceedings, (2007), 1-12. Retrieved from http://journals.tdl.org/icce/index.php/icce/article/view/6479

Zijlema, M., Stelling G. and Smit, P. 2011: SWASH: An operational public domain code for simulating wave fields and rapidly varied flows in coastal waters. Coast. Eng., 58, 992–1012.

APPENDIX A – STOCHASTIC CYCLONE MODEL

Regional tropical cyclone information for the Southern Hemisphere was obtained from the National Climate Centre of the Australian Bureau of Meteorology over the period 1969-2010. Tropical cyclones that feature in multiple agencies' areas have been manually combined in this dataset to provide a "best track". These data contain the coordinates and central pressures of each cyclone throughout its life at mostly 6 hourly intervals. Using these, information about the cyclone direction and speed of movement were derived. To maximize the number of cyclones, while still obtaining a cyclone record that is both representative of the Samoa region while remaining statistically stable, all cyclone tracks were considered that passed within a 6° radius of the coordinate (13.5°S 187.5°E) located midway between Savai'i and Upolu, the two main islands of Samoa.

The frequency of cyclone occurrence is needed to assign a representative time frame over which the synthetic cyclones could have been expected to occur. For the cyclone frequency estimates for the storm surge modelling, a radial limit of 2° (calculated as an area-weighted fraction of the incidence at 6° radius) is used since cyclones whose paths fall outside this radius are not found to produce a storm surge along the coastlines of the two main islands. The cyclone track data were first linearly interpolated to hourly intervals to increase the temporal representation of the cyclone positions throughout their lifetime. Over the 42 cyclone seasons for which cyclone track information was available, six cyclones with central pressure less than 885 hPa travelled within the 2° radius yielding an approximate rate of cyclone occurrence of 1 every 7 years. This is consistent with the analysis of Carter (1987) who estimated that significant cyclones impacting the Western Samoan coast have an average return period of about 7 years (Carter, 1987).

A characteristic of tropical cyclones that is needed to model its wind and pressure field is its size as measured by the radius of maximum winds (RMW). As available cyclone data sets do not contain information on RMW, in this study this parameter was modelled using a bivariate log-linear regression based on Kossin et al. (2007):

$$\mathrm{RMW} = \exp(a_0 + a_1 x_1 + a_2 x_2) \qquad \textbf{(A1)}$$

where x_1 = latitude (in degrees and absolute value), x_2 = minimum central pressure (in hPa) and the coefficients (a_0, a_1, a_2) = (-3.5115, 0.0264, 0.0068) (Kossin, pers. comm. October, 2010). Even though there is a large scatter in the RMW around this central estimate this parameterization of RMW is appropriate for use in the stochastic model used here as it represents a central estimate of this quantity as a function of latitude and intensity, thus incorporating the observed tendency of more intense and lower latitude storms to have a smaller RMW (Vickery et al. 2000; Kimball and Mulekar 2004).

Probability density functions (pdfs) have been widely used to specify the likely distribution of occurrence of variables such as temperature and precipitation (e.g. Wilks, 2011), often in the form of return period curves. Using the 6-hourly cyclone track information, distributions were

developed for cyclone attributes such forward speed, direction of movement, and latitudes and longitudes crossed while the cyclone was within a 6° radius of Samoa on the assumption that the cyclone attributes at any one point in this region were equally likely to occur over Samoa (Fig. A1). The distributions for cyclone direction and speed show that cyclones most commonly approach Samoa from the northwest with a smaller number originating from the northeast. Distributions for month of occurrence were also developed. This was so a random date within a selected cyclone month could be selected so that astronomical tide forcing could be applied to the hydrodynamic simulations.

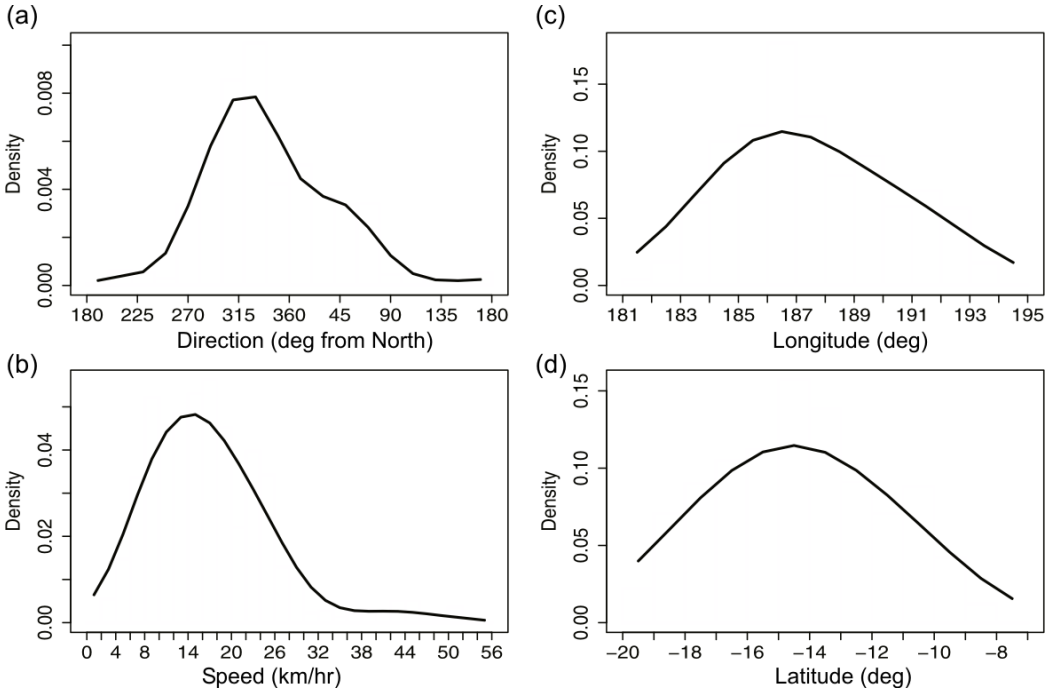

Fig. A.1 Distributions of (a) cyclone direction (b) translation speed (c) crossing longitude (d) crossing latitude of observed cyclones in the Fiji region as well as those occurring during El Niño and La Niña years.

For tropical cyclone intensity, a distribution that has been increasingly employed in the literature is the Generalised Pareto Distribution (GPD) (Coles, 2001). The GPD has a number of advantages for the representation of tropical cyclone intensity, either as measured by central pressure or by wind speed. It is an extreme value distribution and so is able to capture the extreme end of the distribution more effectively. In addition, the GPD is bounded in the sense that at extreme values the cumulative probability distribution becomes asymptotic to 1. This has particular advantages for the representation of tropical cyclone intensities, as theory suggests that there is a maximum tropical cyclone intensity that could occur in a particular climate, beyond which there would be insufficient energy in the climate system to produce stronger storms (e.g. Emanuel, 1987). In this regard, the ability of the GPD to represent an upper bound of intensity as an intrinsic part of the distribution makes it more appropriate for this work than other extreme value distributions that have been employed to represent the observed distribution of tropical cyclone intensities, such as the Gumbel distribution (Coles, 2001; McInnes et al,

2003). To model the cyclone central pressure, the lowest central pressure attained by each cyclone to have occurred within an 8 degree radius of Samoa was selected. This larger region was used to boost the number of sampled cyclones for the GPD fit. The cumulative distribution function (cdf) of the GPD is given by:

$$F(y) = 1 - \left(1 + \frac{\xi(y - \mu)}{\sigma}\right)^{-\frac{1}{\xi}} \quad \textbf{(A2)}$$

where ξ, σ and μ are the shape, scale and threshold parameters respectively. Cyclones whose central pressure attained a value of 885 hPa or lower compared to a climatological average pressure of 1010 hPa (i.e. a pressure deficit of 25 hPa or greater) were selected. The data were best described by a distribution with ξ = -0.604 and σ=46.34. The resultant cumulative distribution curve for cyclones within the 8 degree radius is shown in Fig. A2.

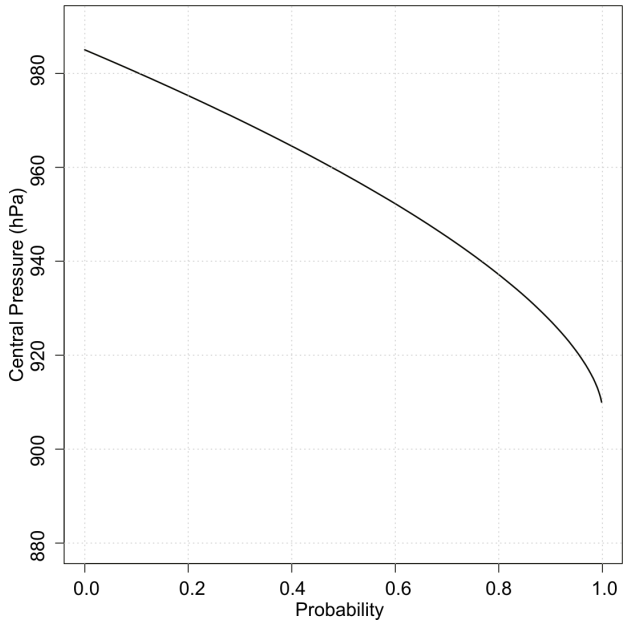

Fig. A.2 Cumulative probability distribution for cyclone central pressure for present climate.

A similar study into tropical cyclone storm tide risk for Fiji has also assessed how changes to tropical cyclone frequency and intensity, projected to occur towards the end of the 21st Century as a result of global warming, may influence storm tide risk (McInnes et al, 2013). A similar assessment of the effect of future tropical cyclone changes on storm tide risk is also under investigation for Samoa but results are not yet available. Therefore, in this study, under future climate conditions it is assumed that cyclone tracks remain unchanged from present conditions. However, we note that the inclusion of future cyclone intensity and frequency changes is not expected to lead to significantly different results to those considered here. This is because McInnes et al., (2013) found that projected cyclone intensity and frequency changes had only a small effect on storm tide return heights associated with return periods of 100 years or shorter in Fiji. A positive effect on storm tide heights was found for return periods typically longer than around 300 years. Assuming that a similar result is found for Samoa, it is therefore unlikely that

future tropical cyclone changes will have a large impact on the 100, 50 and 20-year return heights that are being considered in this study.

A population of 3000 synthetic cyclones was developed for Samoa based on the smoothed empirical distributions for cyclone direction and speed of movement and cyclone position for all cyclone seasons and also for La Nina and El Nino seasons shown in Fig. A1. Cyclone intensity was sampled from the GPD distribution for current climate conditions shown in Fig. A2.

To generate a spatial field of 10-m wind and mean sea level pressure with which to force the hydrodynamic model, the analytical cyclone model of Holland et al. (2010) was implemented in a similar manner as described in Hubert et al. (1991). The revised vortex model of Holland et al. (2010) is an improved version of the earlier radial wind profile model of Holland (1980) in that it uses a different specification of the radial profile to better match both the inner and the outer radial winds in a cyclone. Cyclone intensity is represented by the cyclone's central pressure relative to the background atmospheric pressure, while the size of the cyclone is given by the radius of maximum winds. The initial positions were constrained to fall within a 2º radius of Samoa and the sampled speed and bearing were used to construct a cyclone track by calculating the cyclone's position both forward and back in time across the computational grid of the hydrodynamic model.

APPENDIX B – SAMOA SWAN MODEL

The SWAN model (version 40.91), a phase-averaged solution of the discrete spectral balance of wave-action density (Booij et al., 1999), was selected to estimate archipelago-scale wave fields for this study. Wave-action density (N) is defined as wave energy (E) divided by relative frequency (σ). The propagation of N in time (t), space (x,y), and frequency and direction (σ, θ) is described by:

$$\frac{\partial}{\partial t}N + \frac{\partial}{\partial x}c_x N + \frac{\partial}{\partial y}c_y N + \frac{\partial}{\partial \sigma}c_\sigma N + \frac{\partial}{\partial \theta}c_\theta N = \frac{S_{tot}}{\sigma} \qquad \text{(B1)}$$

In the second and third terms, the velocities c_x and c_y are components of group speed; the third and fourth represent frequency shifting and refraction due to changes in current and depth, respectively; c_σ and c_θ describing the rates of change. The wave field propagation (left side) is balanced by the source terms (S_{tot}) on the right; the source terms are composed of:

$$S_{tot} = S_{in} + S_{wc} + S_{nl4} + S_{fr} + S_{br} + S_{nl3} \qquad \text{(B2)}$$

These individual source terms are wind generation (S_{in}), dissipation (white capping S_{wc}, bottom friction S_{fr}, and breaking S_{br}), and nonlinear interactions (quadruplets S_{nl4} and triads S_{nl3}).

For more information on model formulations and validation of SWAN see Booij et al. (1999) and Ris et al. (1999). Mulligan et al. (2008a, b) provide a succinct overview, including new developments not included in Booij et al. (1999). Hoeke et al. (2011) provides examples of adaptation of the SWAN model to fringing coral reef embayments analogous to those of Apia and other locations in the Samoan islands.

Both the 5 km and 1 km SWAN models are set up on Cartesian grids (see Figs 4 and 8) utilize a spectral discretization of 90 directional bins and 25 logarithmic frequency bins (from 0.042 to 0.411 Hz). In both models, the S_{in} and S_{wc} formulations of Komen et al. (1984) are used. The formulation of Madsen et al. (1988) was used to estimate bottom friction. Wave hydraulic roughness length (kw) scales were set to 0.05 m, approximately in the middle of the range shown appropriate for coral reefs (Hearn, 1999; Lowe et al., 2005). Empirical wave breaking criteria [breaker height coefficient (γb) = 0.9, rate of dissipation coefficient (α) =1] found to be appropriate for coral reefs were used (Hoeke et al. 2013, Filipot and Cheung 2012).

Numerical simulations of wave field conditions during the tropical cyclones were of two types: (1) historical cases and (2) synthetic cases (Figs 4 and 8). For the type 1 historical cases, only the smaller 1 km resolution SWAN grid was used: wave spectra from the global PACCSAP wave hindcast at 1/8 degree intervals were provided along the boundaries with (CFSR or Holland vortex) winds providing input within the grid domain as described above. For the type 2 synthetic cases, both the larger 5 km grid and the smaller 1 km SWAN grid nested within it were used. In this case, no external wave boundary conditions were provided, all wave generation occurred from wind fields within the domain with wave spectra being passed from the 5 km grid to the 1 km grid. Note that the type 2 approach to modelling synthetic cyclone cases could be used to model historical cyclone wave fields (and this was done to inter-compare the two methods), but was not used to define historical wave fields since waves generated by

processes outside the 5 km model domain, e.g. trade-wind or distant storm waves, would not be present.

APPENDIX C – APIA DELFT3D MODEL

The Delft3D modelling system (version 4.00.07.1057M), a coupled wave/circulation model designed for coastal applications (Lesser et al. 2004; Roelvink and Banning 1994), was selected to simulate hydrodynamics during tropical cyclones in this study. The circulation of this so-called "flow" module utilizes a finite-difference solution to the Navier-Stokes equations for unsteady flow on a two-dimensional (2D) or three-dimensional (sigma coordinate system) curvilinear grid; the "wave" module is SWAN, described in the previous section. The forces resulting from total wave dissipation are incorporated as additional surface stresses in the circulation module. The two modules are iteratively coupled so information from the wave module is passed to the flow module to compute wave-induced residual flow and Stokes drift; the subsequent water levels and currents in the circulation module are passed back to the wave module to caluclate an updated wave field. Although this modelling system was developed for use on low-slope sedimentary coastlines, it has been applied with some success to steeper erosional coasts (e.g., Hoeke et al. 2013; Lowe et al. 2009; Mulligan et al. 2008).

All flow module simulations were performed on a 2D curvilinear grid, which varied in spatial resolution from approximately 200m near the northwest and southeast (lateral) boundaries to approximately 10m near the Mulinu'u Penisula and Apia Harbor. The offshore water level boundary was forced by either (1) tidal prediction + sea level anomaly + inverse barometer effect (IBE); or (2) by output points from the Archipelago GCOM2D model at the two offshore boundary corners. In the first case, used for historical runs only, sea level anomaly was provided by either low-pass filtered monthly sea-level values or the CSIRO sea level reconstruction (Church et al. 2004) and IBE calculated from CFSR surface atmospheric pressure. All offshore water level boundaries whether for historical cases or synthetic cyclones, were adjusted to be relative to the 1973 MSL datum. The lateral boundaries were calculated as water-level gradients (Neumann boundary conditions); this forced the components' tidal waves to propagate along the offshore boundary while allowing water levels and current fields to adjust to both the offshore boundary water levels and other (wind and wave) forcing input at the lateral boundaries (Roelvink and Wasltra 2004). The White-Colebrook formulation (Colebrook 1939) was used to estimate bottom boundary layer structure with friction coefficients equivalent to hydraulic roughness length scales of 0.01 m in sandy areas to 0.20 m in reef and hard bottom areas. These values were varied by a factor of 2 as a sensitivity test (see Section 4). Horizontal eddy viscosity was set at 0.5 m^2 s^{-1} based on values observed or used for other coral reefs, in which low sensitivity was found to variations in this parameter (Kraines et al 1998; Lowe et al 2009; Hoeke at al. 2013). Wetting and drying was enabled in the flow module to simulate coastal inundation.

Wave module simulations were performed on the same grid as the flow module, except the wave grid extended 5 grid points in the lateral and 2 grid points in the offshore directions to minimize spurious fluctuations in the flow module due to sudden transitions in wave fields imposed at the wave boundaries. The wave boundary conditions were provided by spectra from the SWAN 1 km model (Appendix B), given at five segments on the offshore boundary. The wave module's set up was the same as for the SWAN models discussed in Appendix B, including the bottom friction formulation.

Uniform wind forcing in both modules was provided by either nearest CFSR grid points or from the GCOM2D model. Bathymetry for both modules' grid was interpolated from the recently acquired Apia LiDAR dataset. An adjustment of water level boundaries to the 1973 MSL datum was performed to ensure that all modelled inundation is relative to the 1973 MSL Datum. This is consistent with the datum of the LiDAR dataset

APPENDIX D – PENINSULA SWASH MODEL

The LiDAR elevation data was used to develop three elevation profiles (low, median and high) that represent the range of bathymetric depths that occur along the reef to the northeast of Mulinu'u Peninsula. The LiDAR bathymetric data were first interpolated to a 1 m resolution. For each meter along the selected transect all elevation values perpendicular to the transect segment up to 50 m either side were extracted, and ranked to define a minimum, average and maximum elevation set (Fig. D1). To remove the irregular reef features the profiles were smoothed with a 20 m moving average filter. Such features are accounted for by an appropriate selection of the roughness coefficient, as described in the next sub-section. The spatial resolution of the LiDAR bathymetry is insufficient to estimate roughness estimates.

The LiDAR survey indicates that the height of the seawall varies along its length. Furthermore, the LiDAR survey heights indicated that for many areas along the sea wall the heights are lower than those specified in JICA (1993). Therefore the representation of the height of the top of the seawall was given two representations in the model: one strictly from those specified in JICA (1993) and the other from maximum LiDAR heights over the seawall area.

Given the lack of observations in Apia to enable model calibration, the approach adopted in this study was to vary the parameter settings within plausible ranges and evaluate the uncertainty associated with the Peninsula mode. Two key parameters that can be varied from the model default values to better describe the conditions being modelled are (1) the bed roughness coefficient, (Manning's coefficient) and (2) wave breaking parameter, α. Two bed roughness coefficients values are used; 0.04 for the most realistic estimate of friction and hence inundation and 0.03 for a smoother coastline and to account for larger inundation. The former is based on the assumption that the transect contains boulders in the sea wall as well as corals whose roughness, as defined by the Manning coefficient, is in the range of 0.04 to 0.07 (Arcement & Schneider, 1989). A value 0.04 is also selected for both the 'optimal parameterization' value and the 'best case' because it represents the lower end of the seawall roughness and the higher end of the reef roughness. The value of 0.03 for the 'worst case' represents a cobble roughness representing the coral reef.

Increasing the value of the breaking parameter increases the threshold surface slope that waves can attain prior to the on-set of breaking, thus delaying wave breaking (Buckley, 2013). Sensitivity runs conducted in this study indicate larger breaking parameters result in larger inundation. In the simulations considered here, three values of α were used, 0.8, 0.9 and 1.0. These values are larger than the default SWASH value of 0.6 for natural beaches but are typical for model studies of steeper fringing reefs (Hoeke et al, 2013b and Buckley 2013).

Other parameters that were varied were the height of the sea wall and the seawall leading slope. The 'worst case' for the sea wall height is 2.4 m (estimated from the LiDAR survey) and the best case is 2.6 m (the specified design height of the seawall; Japan International Cooperation Agency, 1992). Given the recent collection of LiDAR data from which the sea level height has

been estimated, we select an 'Optimal Parameters' value of 2.4 m. A summary of the parameters used by the Peninsula Model is given in Table D1.

Results are presented for four locations along the model profile. The precise locations are determined by the maximum value at model points along a section of the model measured by distance x in a shoreward direction from the offshore origin of the model. The locations are the 'Toe', x = 1430 to 1435, the seawall 'face', x = 1435 to 1440, the top and back of the seawall 'Crest', x = 1445 to 1458 and an inland value '30mInland', x = 1464 to 1479.

Table D1 Summary of parameters used in the SWASH model grouped according to their low to high impact on inundation.

Variable	Optimal Parameters	High Sensitivity (Large inundation)	Low Sensitivity (Small inundation)
Profile	Mean depth profile	Lowest profile (deepest water)	Highest profile (shallowest water)
Friction (Manning's coefficient)	0.04 (USGS, boulders)	0.03 (USGS, cobble)	0.04 (USGS, boulders)
Breaking parameter (α)	0.9	0.8	1.0
Seawall height	2.4 (LiDAR)	2.4 (LiDAR)	2.6 (JICA, 1993)
Seawall leading slope	1:1.7 (LiDAR)	1:1.7 (LiDAR)	1:1.5 (JICA, 1993)

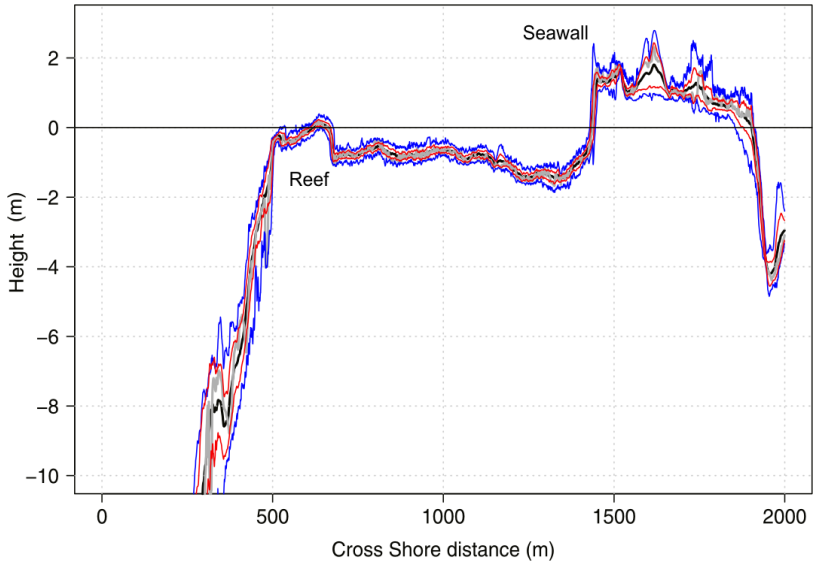

Fig. D.1 Transect analysis of 100m wide strip across the reef and peninsular. Blue lines are the maximum and minimum values of the 200 transects, the black line is the average, the red line is the average plus/minus one standard deviation, while the grey line is the single central transect.

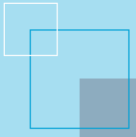

The Centre for Australian Weather and Climate Research is a partnership between CSIRO and the Bureau of Meteorology.